

Contents lists available at ScienceDirect

Petroleum Science

journal homepage: www.keaipublishing.com/en/journals/petroleum-science



Original Paper

Systematic modeling and methodological approaches for optimizing gas storage facility design with fluctuating hydraulic characteristics



Shi-Tao Liu ^a, Cheng-Yu Li ^a, Jun Zhou ^{a, *}, Zi-Chen Li ^a, Zhan-Peng Ye ^a, Jing-Hong Peng ^a, Yun-Xiang Zhao ^b, Guang-Chuan Liang ^{a, **}

- ^a Petroleum Engineering School, Southwest Petroleum University, Chengdu, 610500, Sichuan, China
- ^b Yunnan Provincial Energy Research Institute Co., Ltd., Kunming, 650000, Yunnan, China

ARTICLE INFO

Article history: Received 8 June 2024 Received in revised form 25 December 2024 Accepted 8 April 2025 Available online 11 April 2025

Edited by Teng Zhu

Keywords:
Gas storage
Pipeline diameter optimization
Hybrid genetic algorithm based on
generalized reduced gradient
Multi-condition
Hydraulic characteristics

ABSTRACT

As the proportion of natural gas consumption in the energy market gradually increases, optimizing the design of gas storage surface system (GSSS) has become a current research focus. Existing studies on the two independent injection pipeline network (InNET) and production pipeline network (ProNET) for underground natural gas storage (UNGS) are scarce, and no optimization methods have been proposed yet. Therefore, this paper focuses on the flow and pressure boundary characteristics of the GSSS. It constructs systematic models, including the injection multi-condition coupled model (INM model), production multi-condition coupled model (PRM model), injection single condition model (INS model) and production single condition model (PRS model) to optimize the design parameters. Additionally, this paper proposes a hybrid genetic algorithm based on generalized reduced gradient (HGA-GRG) for solving the models. The models and algorithm are applied to a case study with the objective of minimizing the cost of the pipeline network. For the GSSS, nine different condition scenarios are considered, and iterative process analysis and sensitivity analysis of these scenarios are conducted. Moreover, simulation scenarios are set up to verify the applicability of different scenarios to the boundaries. The research results show that the cost of the InNET considering the coupled pressure boundary is $64.4890 imes 10^4$ CNY, and the cost of the ProNET considering coupled flow and pressure boundaries is 87.7655×10^4 CNY, demonstrating greater applicability and economy than those considering only one or two types of conditions. The algorithms and models proposed in this paper provide an effective means for the design of parameters for GSSS.

© 2025 The Authors. Publishing services by Elsevier B.V. on behalf of KeAi Communications Co. Ltd. This is an open access article under the CC BY-NC-ND license (http://creativecommons.org/licenses/by-nc-nd/

4.0/).

1. Introduction

1.1. Motivation

In the context of the "dual carbon" targets (Jia et al., 2023), natural gas, as a green, clean, and efficient energy source, plays a significant role in the transformation of energy consumption structures. Influenced by the complex and changing international situation, the global natural gas production in 2022 was 4.094 \times 10^{12} m³, with a consumption of 4.061 \times 10^{12} m³, both experiencing

E-mail addresses: zhoujunswpu@163.com (J. Zhou), lgcdjr@163.com (G.-C. Liang).

a slight decline compared to the previous year (IEA, 2023). The "China Natural Gas Development Report (2023)" indicated that in the first half of 2023, China's natural gas production reached 1.155 \times 10¹¹ m³, a year-on-year increase of 5.4%, and the consumption was 1.941 \times 10¹¹ m³, up by 5.6% from the previous year, predicting that natural gas consumption will continue to grow over the next 20 years (Fan et al., 2022). Over the past five years, China's dependency on imported natural gas has consistently exceeded 40% (Du et al., 2023; Wei et al., 2023; Xu et al., 2023), with production far from sufficient to meet consumption. Besides, the issue of natural gas seasonal peak is becoming increasingly prominent, highlighting the importance of using natural gas for emergency and strategic reserves. Underground natural gas storage (UNGS), as one of the main methods of gas storage and peak shaving in the world, play an important role (Zhang G.X. et al., 2017; Zou et al., 2010)

^{*} Corresponding author.

^{**} Corresponding author.

The gas storage system mainly consists of underground storage layers, wells and surface systems. In the gas storage surface system (GSSS), the pipeline networks play a crucial role during operation. It is an important equipment in injection and production conditions, responsible for safely injecting natural gas into the storage and transporting it to the bi-directional gas pipelines. Currently, many studies focus on the underground part of UNGS and the injection and production process, while research on optimizing the design parameters of GSSS is not yet comprehensive. There is widespread concern for the single pipeline network capable of both gas injection and production, yet the research on the two independent injection pipeline network (InNET) and production pipeline network (ProNET) is often neglected. Additionally, in actual production, the control of boundary of flow and pressure at each well are crucial for network stability. The change of conditions and the design parameters of the network interact with each other. To study the effect of changes in well conditions during injection and production processes of GSSS on the design parameters and investment of the pipeline network, and to obtain optimal design parameters with economic efficiency and adaptability, this research work has been conducted.

1.2. Literature review

Current research on UNGS optimization predominantly focuses on the underground components, where numerous studies have been conducted. Scholars often aim to achieve the lowest investment or the best investment strategies during the construction of UNGS. For instance, Zlender and Kravania (2011) established the NLP optimization model OPTUG to obtain optimal costs, Chen et al. (2018) proposed a real option model analyzing the optimal investment strategies for UNGS considering the natural gas market reform or not, and Jelušič et al. (2019) predicted minimum investment and optimal UGS design. Moreover, to ensure the smooth development and operation of UNGS, Wang and Economides (2012) proposed new computational and estimation sequences for monitoring and predicting production rates and durations under the constraints of reduced storage pressures in constructed reservoirs, and Yang et al. (2016) conducted feasibility studies. Zheng et al. (2020) established a geological integrity evaluation system for UNGS geological bodies. To enhance the safety of UNGS operations, Xue et al. (2023) used numerical simulation to predict the maximum storage capacity of the gas storage facility and the variations in pressure and temperature, some scholars have analyzed the integrity failure risks (Zhao et al., 2019) or conducted facility risk analyses (Syed and Lawryshyn, 2020) of UNGS. These studies address technical issues related to the construction of UNGS to achieve economical, efficient, and safe operations. However, there is relatively less in-depth research on GSSS.

In the realm of research on GSSS, Peng et al. (2015) developed a network model and conducted a hydraulic simulation analysis to determine the best seasonal peak scheduling plan for the year. Yu et al. (2018) assessed the reliability of UNGS operations under different injection and production scenarios. Nonetheless, these scholars did not design and study the parameters of GSSS from the perspective of optimization. Zhou et al. (2020) proposed a special genetic algorithm to solve for the model's optimal topology, location of platforms and central stations, pipeline diameters etc. Zhou et al. (2021a, 2021b) focused on optimizing gas storage networks, establishing a mixed-integer nonlinear programming (MINLP) model to find the optimal topology. They considered the affiliation of wells, the number of stations, processing capacity, and flow/ pressure balance in their optimization of the layout and diameter parameters of gas storage surface networks. For flow boundaries, the GSSS under gas production conditions can be categorized into

emergency production condition and peak production condition. For pressure boundaries, the GSSS distinguishes between maximum and minimum pressures under injection and production conditions. Variations in boundaries typically affect the optimization of design parameters for the pipeline network, and conversely, the results of optimizing injection and production pipeline design parameters can impact the efficient operation of the gas storage facility. Although these studies focus on optimizing the design of gas storage surface networks, they do not consider the different boundaries under different conditions. The optimized pipeline diameter parameters may not simultaneously meet the optimal investment under different conditions, which cannot ensure flexibility and safety stability of the UNGS. Our previous work (Zhou et al., 2022) proposed a multi-condition hybrid model that can achieve the lowest investment and optimal design parameters. However, this research was on integrated pipelines network, which did not consider the independent gas injection and production pipe network system. For condensate or oil reservoir-based UNGS, InNET and ProNET arrangements are preferred, such as China's Jing 58. Additionally, this study focuses on the optimization of the parameters under multi-condition, thus considering more comprehensive conditions and resulting in more adaptable optimization outcomes. To summarize, there is no literature currently addressing the parameter optimization of two independent InNET and ProNET by considering the coupling of different conditions.

In addition to focusing on the underground components, to construct a model that closely aligns with the practical design parameters of the GSSS, inspiration can be drawn from optimization models of networks with similar transportation characteristics. For instance, Üster and Dilaveroğlu (2014) designed an optimization model for the periodic expansion of natural gas gathering and transportation network. Wei et al. (2016) targeted the minimal total investment in gas field gathering and transportation network construction by optimizing design parameters such as pipeline diameter and wall thickness. Wang et al. (2018) established a mathematical model to simultaneously optimize gathering and transportation networks and water injection network to reduce investment. Zhou et al. (2018) developed a MINLP model aimed at minimizing investment for natural gas gathering and transportation network. For long-distance natural gas pipelines, Kabirian and Hemmati (2007) created a comprehensive nonlinear optimization model to determine the best design parameters. El-Mahdy et al. (2010) used a genetic algorithm to optimize network parameters and minimize pipeline costs. El-Shiekh (2013) optimized design variables for gas steel pipelines of different diameters and compression ratios to find the optimal design variables. Xue et al. (2024) proposed an integrated model with stable numerical methods for fractured underground gas storage, which contributes to the understanding of optimal design parameters. However, these pipe network systems were optimized under a single condition.

On the other hand, there are various algorithms for optimizing natural gas network design parameters, such as Simulated Annealing (Storn and Price, 1997), Differential Evolution (Babu et al., 2005), Ant Colony Optimization (Chebouba et al., 2009), Particle Swarm Optimization (PSO) (Wu et al., 2014), and Genetic Algorithms (GA) (Srivastava et al., 2015). As research into network optimization problems deepens and design parameter models become increasingly complex, many scholars have begun to improve algorithms to create efficient and fast hybrid algorithms. For example, Zheng and Wu (2012) optimized a natural gas pipeline design parameter model using an improved PSO. Zhou et al. (2015) solved a hot oil pipeline design optimization model using a hybrid algorithm that combines Differential Evolution and PSO. Zhang H.R. et al. (2017) optimized a subsea oil pipeline design parameter model using a multi-swarm cooperative PSO. Liang et al. (2020)

improved the PSO to form a simulated annealing-particle swarm optimization algorithm, obtaining a global optimum for a longdistance pipeline network design parameter model. Among the many optimization algorithms, the optimal solution can be found more efficiently by GA and avoid getting trapped in local optima (Arsegianto et al., 2003; Zhan et al., 2012). Chan et al. (2007) created a hybrid GA by combining it with a local search algorithm to study design parameters of dendritic networks. Tian et al. (2016) proposed an improved parallel cooperative evolutionary GA to optimize parameters like pipeline diameter and wall thickness. Hassan et al. (2020) developed a hybrid GA model (GA-TGA) to solve for the optimal layout design of sewer networks. While many hybrid GA have been successfully used in network design optimization problems, most algorithms have only been applied to longdistance or gathering network design parameter models. However, the GSSS has complex structures and variable conditions. Therefore, this study establishes a Hybrid Genetic Algorithm based on Generalized Reduced Gradient (HGA-GRG) to solve the model for the GSSS. The algorithm efficiently explores the solution space in both continuous and discrete domains. By adaptively using the optimization results from Generalized Reduced Gradient Algorithm (GRG) as the initial population for GA, it accelerates convergence speed and increases the likelihood of finding the global optimum. Furthermore, the algorithm can dynamically adjust the feasible regions for discrete decision variables, allowing it to flexibly respond to changing constraints when addressing the complex design of gas GSSS. This balance of global and local search capabilities enables HGA-GRG to outperform traditional algorithms in tackling complex network design optimization problems.

1.3. Contributions

- (1) This study constructs a set of models for parameter optimization of GSSS, integrating the injection single condition model (INS model), production single condition model (PRS model), injection multi-condition coupled model (INM model), and production multi-condition coupled model (PRM model), with the aim of minimizing the investment in InNET and ProNET.
- (2) By incorporating the fluctuating hydraulic characteristics of the InNET and ProNET, this approach uniquely couples different flow and pressure boundaries under standard single-condition designs.
- (3) The proposed HGA-GRG is capable of solving in both continuous and discrete spaces, ensuring the global optimality of the optimization results.
- (4) Through setting a case and different scenarios, this paper conducts a comparative analysis of the iterative processes and investments for InNET and ProNET and carries out sensitivity analysis of boundaries based on the optimization results
- (5) By establishing simulation scenarios, the applicability and effectiveness of different scenarios are verified.

1.4. Paper organization

Section 2 describes the GSSS. Section 3 establishes the INS model, PRS model, INM model, and PRM model under injection and production conditions. Section 4 introduces the solving algorithm. Section 5 presents case descriptions and scenario settings. Section 6 analyzes the solution results. Section 7 summarizes the paper.

2. System framework

Globally, many countries are currently in the process of constructing UNGS, among which depleted oil and gas reservoir-type UNGSs are the most common. The quality of gas extracted from this kind of UNGS is usually poor, with defects such as wax, sulfur, and water. To prevent the reinjection of residual impurities in the pipelines during the UNGS injection process, causing secondary pollution, these depleted reservoir-type UNGSs usually adopt separate network layouts for injection and production. Unlike traditional oil and gas field surface networks, the changing conditions of injection and production gases lead to significant differences in well flow and pressure. Therefore, this study optimizes the parameters of the InNET and ProNET suitable for various conditions. The research approach is illustrated in Fig. 1.

2.1. Characteristics of GSSS

The well flow properties in production directly influence the priority setting method for pipelines. For UNGS in condensate or oil reservoirs, the well flow at the beginning often consists of three phases: oil, gas, and water. Hence, the pipelines may experience low-temperature condensation or wax deposition. Additionally, if the pipelines are not thoroughly cleaned at the beginning of the production phase, corrosive impurities in the pipelines can be injected underground along with the dry gas during the injection phase, causing secondary pollution to the formation and adversely affecting the lifespan of the facility. Therefore, for UNGS in condensate or oil reservoirs, two independent pipeline network are used preferred.

Two sets of pipeline network are required for gas injection and production, as indicated in Fig. 2. For partial wells, gas injection and production are all in one well. The pipelines from I_1 to I_2 are for gas injection, and from J_1 to J_2 are for gas production. For other wells which can only be used for gas injection or production, the pipelines from I_3 to I_4 are for gas injection, and from J_3 to J_4 are for gas production. Therefore, unlike conventional oil and gas field that only consider ProNET, the GSSS need to account for an additional set of InNET.

2.2. Design of InNET and ProNET

A traditional design process for a GSSS is shown in Fig. 3. The process starts by defining the UNGS's function orientation, predicting downstream natural gas demand to determine the monthly uneven coefficient, and calculating the seasonal peak volume and the emergency volume for non-interruptible customers to determine the peak volume. By determining the topology and pipeline materials of pipeline networks, the pipeline design parameters are calculated and selected, followed by simulation verification. Finally, if the network parameters do not meet hydraulic constraints, they are adjusted until they do, at which output the design results of pipeline networks.

2.2.1. UNGS capacity

Generally, UNGSs are established mainly as seasonal peak reserves and emergency reserves for users. Therefore, calculating the economically reasonable seasonal peak and emergency volumes is crucial for determining the capacity of the UNGS. The determination of UNGS capacity can be divided into calculations based on the unevenness coefficient, calculations according to natural gas management regulations, and the capacity determined by field surveys.

The injection capacity of the UNGS can be obtained based on the peak volume of the UNGS and the number of injection days, as

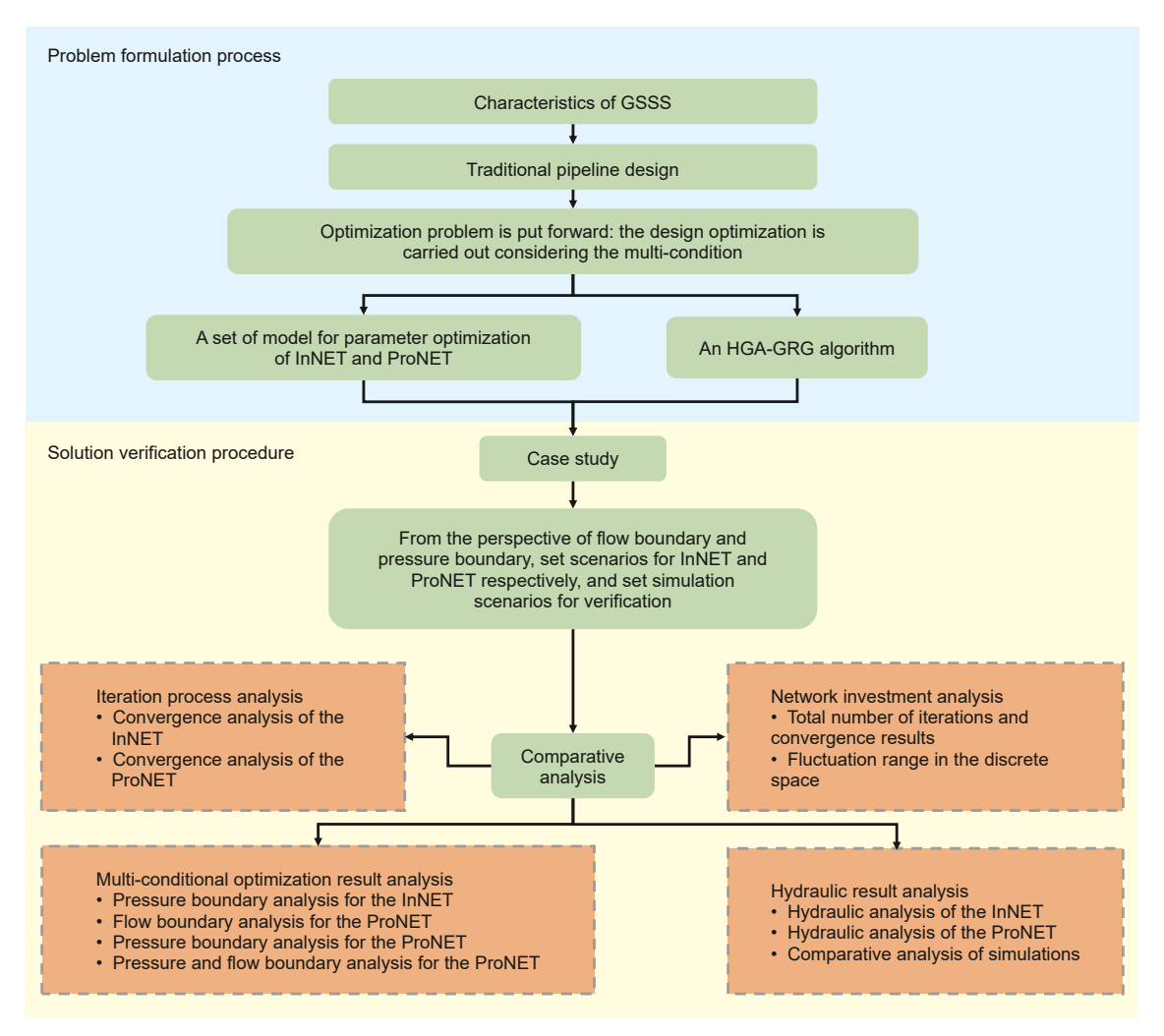


Fig. 1. Research approach.

shown in Eq. (1). The production capacity of the UNGS is calculated according to Eq. (2), with the emergency production capacity calculated as shown in Eq. (3), and the peak production capacity as shown in Eq. (4).

$$Q^{IC} > \frac{V^{PPC}}{t^{IC}} \tag{1}$$

$$Q^{PC} > \max \left[Q^{EPC}, Q^{PPC} \right]$$
 (2)

$$Q^{EPC} = \frac{V^{EPC}}{t^{EPC}} \tag{3}$$

$$Q^{PPC} = \frac{V^{PPC}}{t^{PPC}} \tag{4}$$

where $Q^{\rm IC}$ is the injection capacity of UNGS, ${\rm m}^3/{\rm d.}~V^{\rm PPC}$ is the peak production volume, ${\rm m}^3.~t^{\rm IC}$ is the number of injection days, d. $Q^{\rm PC}$ is the production capacity of UNGS. $Q^{\rm EPC}$ is the emergency production capacity of UNGS, ${\rm m}^3/{\rm d.}~Q^{\rm PPC}$ is the peak production capacity of UNGS, ${\rm m}^3/{\rm d.}~V^{\rm EPC}$ is the emergency production volume, ${\rm m}^3.~t^{\rm EPC}$ is the number of emergency production days, d. $t^{\rm PPC}$ is the number of peak production days, d.

2.2.2. Well injection and production capacity

While the injection and production capacity of an individual well is typically determined early in the drilling engineering process based on the optimization of the tubing, the well technology's impact on adjusting the flow rates necessitates the design of individual well capacities. The design injection capacity of a well is as shown in Eq. (5), and the production capacity of a well as shown in Eq. (6).

$$q^{\rm IC} = \frac{Q^{\rm IC}}{N_i^{\rm IC}} \tag{5}$$

$$q^{\rm PC} = \frac{Q^{\rm PC}}{N_i^{\rm PC}} \tag{6}$$

where $q^{\rm IC}$ is the injection capacity per well, m³/d. $N_i^{\rm IC}$ is the number of injection wells, seats. $q^{\rm PC}$ is the production capacity per well, m³/d. $N_i^{\rm PC}$ is the number of production wells, seats.

2.2.3. Pipeline layout and pipeline size

The topology of the GSSS is determined based on the type of UNGS, the quality of the gas stored, and the distribution of wells. Pipelines should be made from materials with high strength, good

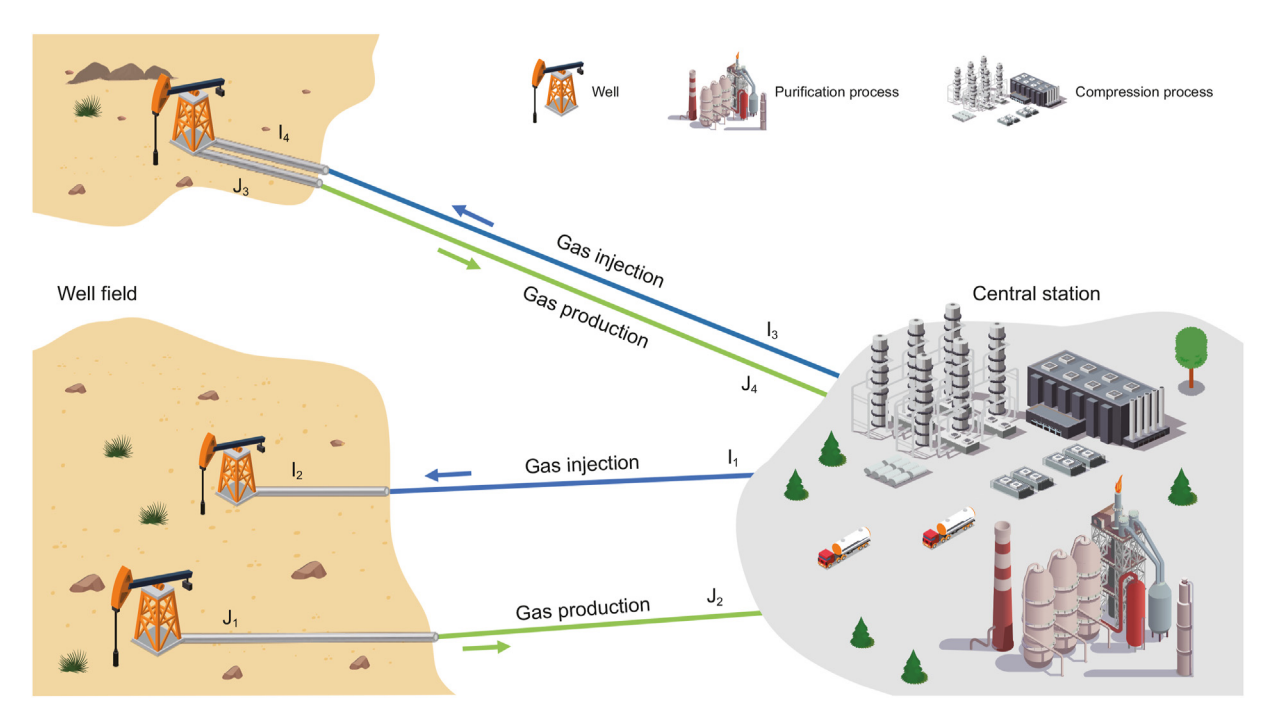


Fig. 2. Schematic diagram of well field pipelines.

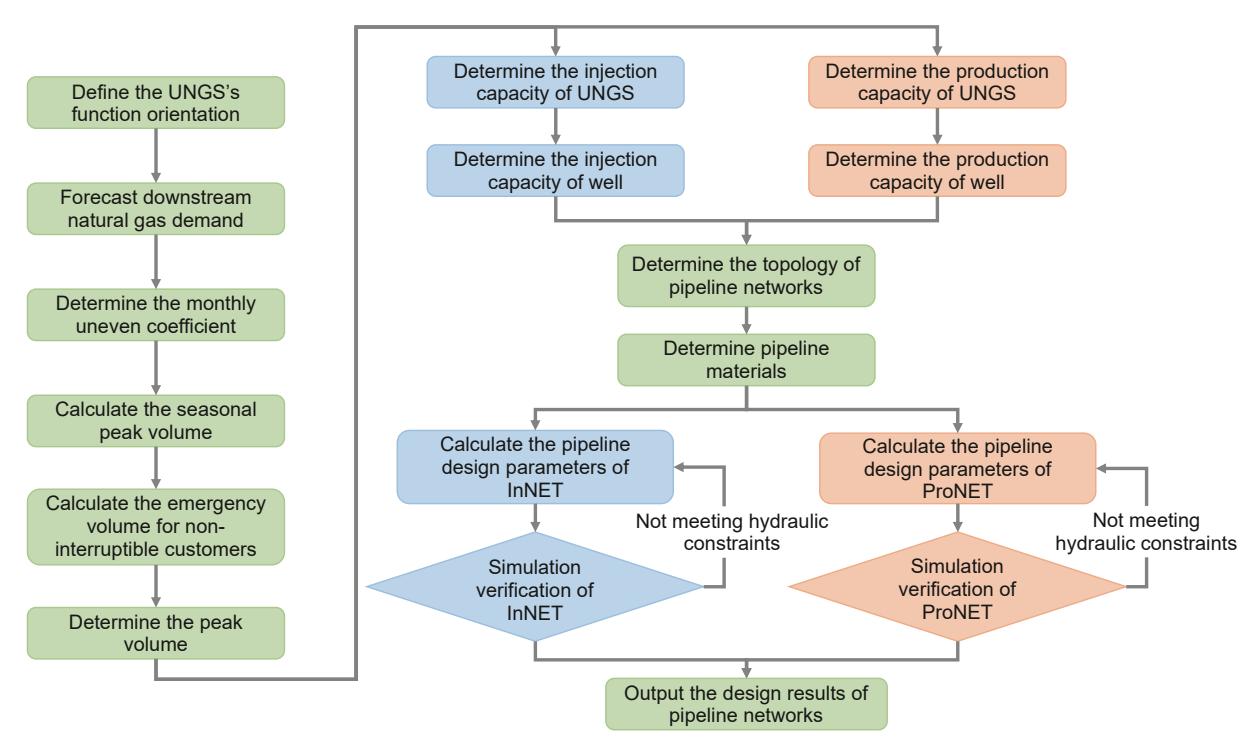


Fig. 3. Flowchart of traditional GSSS design.

plasticity and toughness, good weldability and corrosion resistance. Additionally, the materials should be easy to process and manufacture while also being cost-effective. The grade of the steel is mainly determined based on the pressure, temperature, and characteristics of the transported medium. The flow rate of traditional pipeline is calculated as shown in Eq. (7). The pipeline wall thickness is calculated using Eq. (8).

$$q_{\nu} = 5033.11(10d)^{\frac{8}{3}} \sqrt{\frac{P_1^2 - P_2^2}{\Delta ZTL}}$$
 (7)

$$\eta = \frac{PD}{2R\phi E\sigma_T} + C \tag{8}$$

where q_v is the pipeline flow, m^3/d . d is the pipeline inner diameter,

mm. P_1 is the starting pressure of pipeline, MPa. P_2 is the ending pressure of pipeline, MPa. Δ is the relative gas density. Z is the compressibility coefficient of gas at average pressure and temperature. T is the average thermodynamic temperature of gas, K. L is the length of pipeline, km. η is the wall thickness of pipeline, mm. P is the design pressure of pipeline, MPa. D is the diameter of pipeline, mm. R is the minimum yield strength, MPa. ϕ is the strength design coefficient. E is the axial joint coefficient. σ_T is the temperature reduction coefficient, σ_T to be taken as 1.0 when temperature is below 120 °C. C is the corrosion allowance, 2.0 mm.

2.3. Description of the optimization problem

Compared to the design of conventional gas field surface networks, GSSS require an additional injection process. These networks of GSSS demand higher safety requirements and longer life cycles, making the reduction of the InNET and ProNET investment a primary research focus.

2.3.1. Fluctuating hydraulic characteristic

As shown in Fig. 4, the GSSS undergoes annual variations from "well production pressure upper limit to lower limit" and "well injection pressure lower limit to upper limit." Thus, traditional designs often use the well's upper pressure limit as the network's maximum design pressure requirement, using the maximum flow as the design requirement for the pipeline's capacity. This method is theoretically applicable to maximum operating conditions. However, in practical applications, when the well pressure or flow is low, the driving force for flow becomes insufficient, which may result in designed network parameters failing to satisfy hydraulic conditions such as flow velocities, thereby impacting the overall efficiency of the system. Furthermore, low pressure can also lead to flow that do not meet operational requirements, further affecting the performance of the pipeline network.

This paper establishes INM model and PRM model for InNET and ProNET respectively, forms INS model and PRS model at the same time, and carries out optimization solution and comparative analysis through the designed algorithm. In past engineering practices, the maximum flow and maximum pressure boundaries were often

used for network parameter design. In this paper, INS model and PRS model only consider one condition. For example, for the Pro-NET, only one flow boundary and one pressure boundary are taken into account. In contrast, INM model and PRM model integrate the flow and pressure boundaries, enabling the optimized network parameters to simultaneously meet multiple conditions.

2.3.2. Known data description

- (1) Pipeline sets: injection pipeline set, denoted as A^{IC} , with elements $z \in A^{IC} = \{1, 2, ..., N_z\}$; production pipeline set, denoted as A^{PC} , with elements $o \in A^{PC} = \{1, 2, ..., N_o\}$.
- (2) Node sets: well node set, denoted as W, with elements $i \in W = \{1, 2, ..., N_i\}$; platform node set, denoted as B, with elements $j \in B = \{1, 2, ..., N_j\}$; central station node set, denoted as G, with elements $k \in G = \{1, 2, ..., N_k\}$.
- (3) Node parameters: design injection and production capacities for well; gas temperature at the central station; gas pressure at the central station; gas temperature at the ProNETwell; gas pressure at the ProNET well.
- (4) Pipeline parameters: relative density of natural gas; design pressure for pipelines; minimum yield strength for pipelines; axial joint coefficient for pipelines; strength design coefficient for pipelines; material performance coefficient for selecting pipeline materials; diameter and wall thickness design parameters are listed in Table S1 in supporting material; maximum and minimum pressures for the networks; economic flow velocity range for pipelines.

2.3.3. Solution description

- (1) Algorithm: iterative process.
- (2) Investment: each pipeline investment of the InNET and ProNET.
- (3) Pipeline parameters: internal diameter, wall thickness of each pipeline in the InNET and ProNET, inlet and outlet flow velocities and pressures for each pipeline.

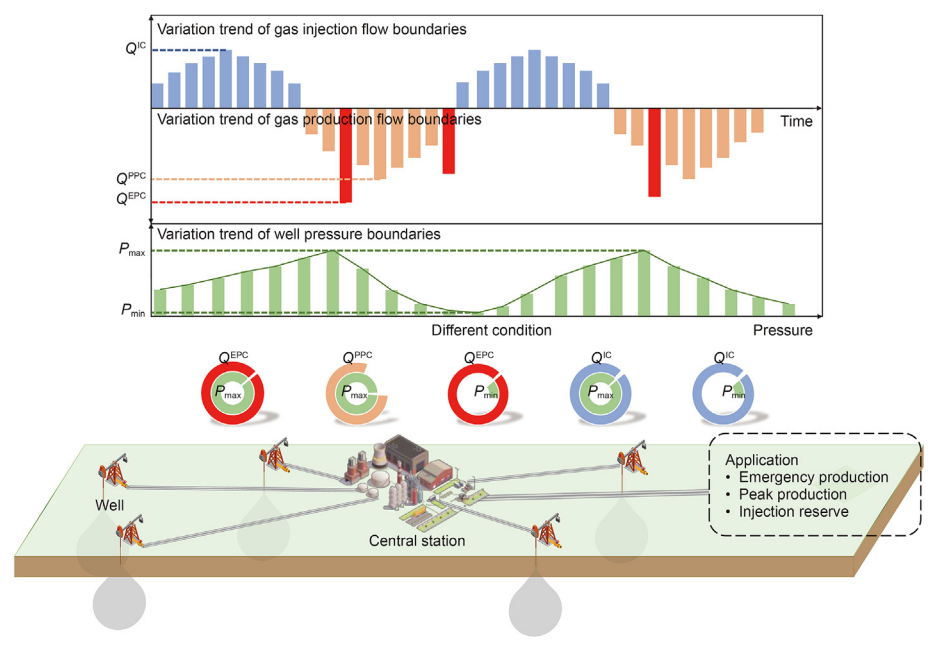


Fig. 4. Diagram of injection and production condition variations.

3. Optimization model

The problem of optimizing design parameters can be transformed into independent optimization problems for the InNET and ProNET. INM model and PRM model are proposed respectively. On this basis, the INS model and the PRS model, which only consider one condition, are formed respectively.

3.1. Objective function

The total investment is represented as Eq. (9), where the cost of the InNET is given by Eq. (10), and the cost of the ProNET is given by Eq. (11). In addition, this paper introduces a set of conditions, X, with $x \in X$, and the number of conditions is set as n.

$$\min F = F^{\mathsf{IC}} + F^{\mathsf{PC}} \tag{9}$$

where F is the total investment of network, CNY. F^{IC} is the investment of InNET, CNY. F^{PC} is the investment of ProNET, CNY.

$$F^{IC} = \frac{1}{n} \sum_{x \in X} \sum_{z \in AlC} \frac{\pi}{4} \left(d_{z,x} + D_{z,x} \right) \eta_{z,x} L_z \rho_s f_s \tag{10}$$

$$F^{PC} = \frac{1}{n} \sum_{x \in X_0} \sum_{e \in A^{PC}} \frac{\pi}{4} \left(d_{o,x} + D_{o,x} \right) \eta_{o,x} L_o \rho_s f_s \tag{11}$$

where $d_{z,x}$ is the inner diameter of injection pipeline z under condition x, mm. $D_{z,x}$ is the diameter of injection pipeline z under condition x, mm. $\eta_{z,x}$ is the wall thickness of injection pipeline z under condition x, mm. L_z is the length of injection pipeline z, km. ρ_s is the density of steel, kg/m³. f_s is the price of steel, CNY/kg. $d_{o,x}$ is the inner diameter of production pipeline o under condition x, mm. $D_{o,x}$ is the diameter of production pipeline o under condition x, mm. $\eta_{o,x}$ is the wall thickness of production pipeline o under condition x, mm. L_o is the length of production pipeline o, km.

3.2. Constraints

3.2.1. Node flow balance constraints

For the InNET, the gas flow in pipeline (j,i) between platform node j and well node i equals the injection flow of well node i connected to this pipeline, as shown in Eq. (12).

$$a_{j,i} \cdot q_{i,x}^{\text{IC}} = Q_{ji,x}^{\text{IC}} \quad \forall i \in W, \forall j \in B, \forall x \in X$$
 (12)

where $a_{j,i}$ is the connection coefficient between platform node j and well node i, connected if $a_{j,i} = 1$, otherwise $a_{j,i} = 0$. $q_{i,x}^{\rm IC}$ is the injection flow of well node i under condition x, m^3/d . $Q_{j,x}^{\rm IC}$ is the gas flow of injection pipeline (j,i) under condition x, m^3/d .

Given the injection flow for all pipelines (j,i), the injection flow at each platform node j is the sum of all pipeline flows connected to the well node i and the platform node j, as shown in Eq. (13).

$$\sum_{j \in B} a_{j,i} \cdot Q_{ji,x}^{IC} = q_{j,x}^{IC}$$

$$\tag{13}$$

where $q_{j,x}^{\rm IC}$ is the injection flow of platform node j under condition x, m^3/d .

For the InNET, the flow in pipeline (k,i) between central station node k and well node i equals the injection flow of well node i connected to this pipeline, as shown in Eq. (14). The flow in pipeline (k,j) between central station node k and platform node j equals the injection flow of platform node j connected to this pipeline, as

shown in Eq. (15).

$$a_{k,i} \cdot q_{i,x}^{\text{IC}} = Q_{ki,x}^{\text{IC}} \quad \forall i \in W, \forall k \in G, \forall x \in X$$
 (14)

$$a_{k,j} \cdot q_{i,x}^{IC} = Q_{ki,x}^{IC} \quad \forall i \in W, \forall k \in G, \forall x \in X$$
 (15)

where $a_{k,i}$ is the connection coefficient between central station node k and well node i, connected if $a_{k,i} = 1$, otherwise $a_{k,i} = 0$. $Q_{ki,x}^{IC}$ is the gas flow of injection pipeline (k,i) under condition x, m^3/d . $a_{k,j}$ is the connection coefficient between central station node k and platform node j, connected if $a_{k,j} = 1$, otherwise $a_{k,j} = 0$. $Q_{kj,x}^{IC}$ is the gas flow of injection pipeline (k,j) under condition x, m^3/d .

The injection flow at central station node k is the sum of all gas flows in pipelines connected to this central station, which is also equal to the sum of all injection flows from well nodes i, as shown in Eq. (16).

$$\begin{split} \sum_{i \in W} a_{k,i} \cdot Q_{ki,x}^{IC} + \sum_{j \in B} a_{k,j} \cdot Q_{kj,x}^{IC} &= \sum_{i \in W} q_{i,x}^{IC} \\ &= q_{k,x}^{IC} \quad \forall i \in W, j \in B, \, \forall k \in G, \, \forall x \in X \end{split}$$

$$(16)$$

where $q_{k,x}^{\text{IC}}$ is the injection flow of central station node k under condition x. m^3/d .

Based on the flow balance constraints of the InNET, represented by Eq. (12)—(16), the flow balance constraints for the ProNET can be similarly defined. The production flow in pipeline (i,j) between well node i and platform node j equals the production flow of the well node, as shown in Eq. (17). The production flow at platform node j is as shown in Eq. (18). Considering the gas flow of pipelines between well node i, platform node j, and central station node k, as given by Eq. (19) and Eq. (20), the production flow at central station node k is as shown in Eq. (21).

$$a_{i,i} \cdot q_{i,x}^{PC} = Q_{ii,x}^{PC} \quad \forall i \in W, \forall j \in B, \forall x \in X$$
 (17)

$$\sum_{i \in R} a_{j,i} \cdot Q_{ij,x}^{PC} = q_{j,x}^{PC}$$
 (18)

$$a_{k,i} \cdot q_{i,x}^{PC} = Q_{ik,x}^{PC} \quad \forall i \in W, \forall k \in G, \forall x \in X$$

$$\tag{19}$$

$$a_{k,j} \cdot q_{i,x}^{PC} = Q_{ik,x}^{PC} \quad \forall i \in W, \forall k \in G$$
 (20)

$$\sum_{i \in \mathcal{W}} q_{i,x}^{\text{PC}} = q_{k,x}^{\text{PC}} \quad \forall i \in \mathcal{W}, \forall k \in G$$
 (21)

where $q_{i,x}^{PC}$ is the production flow of well node i under condition x, m^3/d . $Q_{ij,x}^{PC}$ is the gas flow of production pipeline (i,j) under condition x, m^3/d . $Q_{j,x}^{PC}$ is the production flow of platform node j under condition x, m^3/d . $Q_{ik,x}^{PC}$ is the gas flow of production pipeline (i,k) under condition x, m^3/d . $Q_{jk,x}^{PC}$ is the gas flow of production pipeline (j,k) under condition x, m^3/d . q_k^{PC} is the production flow of central station node k under condition x, m^3/d .

3.2.2. Economic flow velocity constraints

To ensure that the flow velocity within the economic range, constraints are placed on the flow velocity for both the InNET and ProNET, as shown in Eq. (22) and Eq. (23).

$$v_{z,\min} \le v_{z,x} \le v_{z,\max} \quad \forall z \in A^{IC}$$
 (22)

$$v_{o,\min} \le v_{o,x} \le v_{o,\max} \quad \forall o \in A^{PC}$$
 (23)

where $v_{z,\min}$ is the minimum allowable flow velocity of injection pipeline z, m/s. $v_{z,x}$ is the flow velocity of injection pipeline z under condition x, m/s. $v_{z,\max}$ is the maximum allowable flow velocity of injection pipeline z, m/s. $v_{o,\min}$ is the minimum allowable flow velocity of production pipeline o under condition x, m/s. $v_{o,x}$ is the flow velocity of production pipeline o, m/s. $v_{o,\max}$ is the maximum allowable flow velocity of production pipeline o, m/s.

3.2.3. Pipeline wall thickness constraints

The cost of the pipeline is closely related to its wall thickness and is also influenced by the design pressure, minimum yield strength, strength design coefficient, and axial joint coefficient. The wall thickness of each pipeline in the InNET must meet the constraints, as shown in Eq. (24), and the wall thickness of each pipeline in the ProNET must meet the constraints, as shown in Eq. (25).

$$\eta_{z,x} \ge \frac{P_z D_{z,x}}{2R\phi E\sigma_T} \quad \forall z \in A^{\text{IC}}, \, \forall x \in X$$
(24)

$$\eta_{o,x} \ge \frac{P_o D_{o,x}}{2R\phi E\sigma_T} \quad \forall o \in A^{PC}, \forall x \in X$$
(25)

where P_Z is the design pressure of injection pipeline z, MPa. P_0 is the design pressure of production pipeline o, MPa.

3.2.4. Pipeline diameter constraints

Considering that the wall thickness and internal diameter are discrete variables and that the pipeline specifications need to meet the existing pipeline sets available on the market, constraints for the external diameter of the InNET are as shown in Eq. (26), and for the ProNET as shown in Eq. (27). Furthermore, all diameters must exist within the set of available external diameters, as stated in Eq. (28).

$$D_{z,x} = d_{z,x} / 10 + 2\eta_{z,x} \quad \forall z \in A^{IC}, \forall x \in X$$
 (26)

$$D_{o,x} = d_{o,x} / 10 + 2\eta_{o,x} \quad \forall o \in A^{PC}, \forall x \in X$$
(27)

$$D_{z,x}, D_{o,x} \in H \quad \forall z \in A^{IC}, \forall o \in A^{PC}, \forall x \in X$$
 (28)

where H is the external diameter set.

3.2.5. Node pressure constraints

The pressure at each well node i, platform node j, and central station node k in both InNET and ProNET must remain within specified pressure limits, resulting in node pressure constraints as shown in Eq. (29) and Eq. (30).

$$p_{\min}^{IC} \le p_{i,x}^{IC}, p_{j,x}^{IC}, p_{k,x}^{IC} \le p_{\max}^{IC} \quad \forall i \in W, \forall j \in B, \forall k \in G, \forall x \in X$$
(29)

 $p_{\min}^{\text{PC}} \le p_{i,x}^{\text{PC}}, p_{j,x}^{\text{PC}}, p_{k,x}^{\text{PC}} \le p_{\max}^{\text{PC}} \quad \forall i \in W, \forall j \in B, \forall k \in G, \forall x \in X$ (30)

where p_{\min}^{IC} is the minimum allowable pressure of the InNET nodes, $p_{i,x}^{IC}$ is the pressure of InNET well node i under condition x, $p_{j,x}^{IC}$ is the pressure of InNET platform node j under condition x, $p_{k,x}^{IC}$ is the pressure of InNET central station node k under condition x, and p_{max}^{IC} is the maximum allowable pressure of the InNET nodes, MPa. p_{min}^{PC} and p_{max}^{PC} is the minimum and maximum allowable pressures of the ProNET nodes, respectively, MPa. $p_{i,x}^{PC}$, $p_{j,x}^{PC}$, and $p_{k,x}^{PC}$ are respectively the pressures of ProNET well node i, platform node j, and central station node k under condition x.

3.2.6. Pipeline pressure drop constraints

For gas transporting from starting point 1 to endpoint 2, the pressure balance constraints are as shown in Eq. (31) and Eq. (32).

$$p_{z,1,x}^2 - p_{z,2,x}^2 = \frac{L_z}{d_{z,x}^5} K_{z,x} Q_{z,x}^2 \quad \forall z \in A^{\text{IC}}, \forall x \in X$$
 (31)

$$p_{0,1,x}^2 - p_{0,2,x}^2 = \frac{L_o}{d_{0,x}^5} K_{0,x} Q_{0,x}^2 \quad \forall o \in A^{PC}, \forall x \in X$$
 (32)

where $p_{z,1,x}$ is the starting pressure of injection pipeline z under condition x, MPa. $p_{z,2,x}$ is the ending pressure of injection pipeline z under condition x, MPa. $K_{z,x}$ is the hydraulic coefficient of injection pipeline z under condition x. $Q_{z,x}$ is the gas flow of injection pipeline z under condition x, m^3/d . $p_{o,1,x}$ is the starting pressure of production pipeline s0 under condition s1, MPa. s2, is the ending pressure of production pipeline s3 under condition s4. MPa. s4, is the hydraulic coefficient of production pipeline s5 under condition s6, s7, is the gas flow of production pipeline s8 under condition s8, s9, s9, is the gas flow of production pipeline s9 under condition s8, s9, s9,

The hydraulic coefficients $K_{Z,X}$ and $K_{O,X}$, which are determined by the friction coefficient, compression coefficient, gas temperature, and relative gas density, are described in Eq. (33) and Eq. (34).

$$K_{z,x} = \frac{\lambda_z \cdot Z_z \cdot T_z \cdot \Delta_z}{0.0129^2} \quad \forall z \in A^{\text{IC}}, \forall x \in X$$
 (33)

$$K_{o,x} = \frac{\lambda_o \cdot Z_o \cdot T_o \cdot \Delta_o}{0.0129^2} \quad \forall o \in A^{PC}, \forall x \in X$$
 (34)

where λ_Z is the hydraulic friction coefficient of injection pipeline z. Z_Z is the compression coefficient of injection pipeline z. T_Z is the average gas temperature of injection pipeline z, K. Δ_Z is the relative gas density of injection pipeline z. λ_0 is the hydraulic friction coefficient of production pipeline o. Z_0 is the compression coefficient of production pipeline o. T_0 is the average gas temperature of production pipeline o, T_0 is the relative gas density of production pipeline o.

3.3. Models' discussion

This section introduces the PRM model, PRS model, INM model and INS model. Among them, PRM model and INM model integrate multi-condition to obtain a set of pipeline parameters. PRS model and INS model are formed on the basis of PRM model and INM model, and they only consider one condition.

3.3.1. PRM model and PRS model

In the PRM model, pipelines optimized for different conditions must have the same inner diameter and wall thickness. Thus, constraints for the inner diameter and wall thickness of pipelines under different conditions are given by Eq. (35) and Eq. (36), respectively.

$$d_{0,x} = \frac{1}{n} \sum_{x \in X} d_{0,x} \quad \forall o \in A^{PC}$$

$$(35)$$

$$\eta_{o,x} = \frac{1}{n} \sum_{x \in X} \eta_{o,x} \quad \forall o \in A^{PC}$$
(36)

As the PRM model solves for the ProNET under n conditions by coupling, its objective function is the investment of a single network, as shown in Eq. (37). When considering only one type condition independently in the ProNET, with n=1, it is referred to as the PRS model.

$$\min F^{\text{PC}} = \frac{1}{n} \sum_{x = X_0 = A^{\text{PC}}} \frac{\pi}{4} (d_{o,x} + D_{o,x}) \eta_{o,x} L_o \rho_s f_s$$

$$a_{j,i} \cdot q_{i,x}^{PC} = Q_{ij,x}^{PC} \quad \forall i \in W, \forall j \in B, \forall x \in X$$

$$a_{k,i} \cdot q_{i,x}^{PC} = Q_{ik,x}^{PC} \quad \forall i \in W, \forall k \in G, \forall x \in X$$

$$a_{k,j} \cdot q_{j,x}^{PC} = Q_{jk,x}^{PC} \quad \forall i \in W, \forall k \in G, \forall x \in X$$

$$\sum_{j \in B} a_{j,i} \cdot Q_{ij,x}^{PC} = q_{j,x}^{PC}$$

$$\sum_{j \in B} q_{i,x}^{PC} = q_{k,x}^{PC} \quad \forall i \in W, \forall k \in G, \forall x \in X$$

$$v_{o,\min} \leq v_{o,x} \leq v_{o,\max} \quad \forall o \in A^{PC}, \forall x \in X$$

$$v_{o,\min} \leq v_{o,x} \leq v_{o,\max} \quad \forall o \in A^{PC}, \forall x \in X$$

$$d_{o,x} \geq \frac{P_{o}D_{o,x}}{2R\phi E\sigma_{T}} \quad \forall o \in A^{PC}$$

$$d_{o,x} = \frac{1}{n} \sum_{x \in X} d_{o,x} \quad \forall o \in A^{PC}$$

$$\eta_{o,x} = \frac{1}{n} \sum_{x \in X} \eta_{o,x} \quad \forall o \in A^{PC}$$

$$D_{o,x} \in H \quad \forall o \in A^{PC}, \forall x \in X$$

$$p_{\min}^{PC} \leq p_{i,x}^{PC}, p_{j,x}^{PC}, p_{k,x}^{PC} \leq p_{\max}^{PC} \quad \forall i \in W, \forall j \in B, \forall k \in G, \forall x \in X$$

$$p_{o,1,x}^{PC} = p_{o,2,x}^{PC} = \frac{L_{o}}{d_{o,x}^{PC}} K_{o,x} Q_{o,x}^{PC} \quad \forall o \in A^{PC}, \forall x \in X$$

3.3.2. INM model and INS model

Based on the PRM model, as represented by Eq. (37), the INM model for the gas InNET is constructed, as shown in Eq. (38). When considering only one type of flow boundary and one type of pressure boundary independently in the InNET, with n=1, it is referred to as the INS model.

$$\min F^{\text{IC}} = \frac{1}{n} \sum_{x \in X_Z \in A^{\text{IC}}} \frac{\pi}{4} \left(d_{z,x} + D_{z,x} \right) \eta_{z,x} L_z \rho_s f_s$$

$$\begin{cases} a_{j,i} \cdot q_{i,x}^{lC} = Q_{j,x}^{lC} \quad \forall i \in W, \forall j \in B, \forall x \in X \\ a_{k,i} \cdot q_{i,x}^{lC} = Q_{ki,x}^{lC} \quad \forall i \in W, \forall k \in G, \forall x \in X \\ a_{k,j} \cdot q_{j,x}^{lC} = Q_{kj,x}^{lC} \quad \forall i \in W, \forall k \in G, \forall x \in X \\ \sum_{j \in B} a_{j,i} \cdot Q_{j,x}^{lC} = q_{j,x}^{lC} \\ \sum_{j \in W} q_{i,x}^{lC} = q_{k,x}^{lC} \quad \forall i \in W, \forall k \in G, \forall x \in X \\ v_{z,\min} \leq v_{z,x} \leq v_{z,\max} \quad \forall z \in A^{lC}, \forall x \in X \\ v_{z,\min} \leq v_{z,x} \leq v_{z,\max} \quad \forall z \in A^{lC}, \forall x \in X \\ d_{z,x} \geq \frac{P_z D_{z,x}}{2R\phi E\sigma_T} \quad \forall z \in A^{lC} \\ d_{z,x} = \frac{1}{n} \sum_{x \in X} d_{z,x} \quad \forall z \in A^{lC} \\ \eta_{z,x} = \frac{1}{n} \sum_{x \in X} \eta_{z,x} \quad \forall z \in A^{lC} \\ D_{z,x} \in H \quad \forall z \in A^{lC}, \forall x \in X \\ p_{min}^{lC} \leq p_{i,x}^{lC}, p_{j,x}^{lC}, p_{k,x}^{lC} \leq p_{max}^{lC} \quad \forall i \in W, \forall j \in B, \forall k \in G, \forall x \in X \\ p_{z,1,x}^{2} - p_{z,2,x}^{2} = \frac{L_z}{d_{z,x}^{5}} K_{z,x} Q_{z,x}^{2} \quad \forall z \in A^{lC}, \forall x \in X \end{cases}$$

$$(38)$$

4. Optimization method

4.1. Optimization framework

To address the challenges and models described, this study establishes HGA-GRG algorithm. The optimization framework is illustrated in Fig. 5.

4.2. Algorithm

The Genetic Algorithm (GA) is a metaheuristic search method inspired by Darwinian natural selection and genetic evolution (Zhang and Liu, 2017). First introduced by Goldberg in 1987 to optimize natural gas pipelines (Deb et al., 2002), GA is widely recognized for its high likelihood of finding global optima (Arai et al., 2009; Zhan et al., 2012), though it does not guarantee global optimality in all cases. Its primary advantage lies in its ability to directly handle discrete pipeline sizes and effectively track optimal solutions (El-Mahdy et al., 2010). However, GA is limited by challenges in efficiency and precision. The Generalized Reduced Gradient (GRG) algorithm, originally proposed by Abadie and Carpentier and further developed by Lasdon in the 1970s (Abadie and Carpentier, 1969), extends linear optimization methods to nonlinear constraints. GRG simplifies constrained problems by

(37)

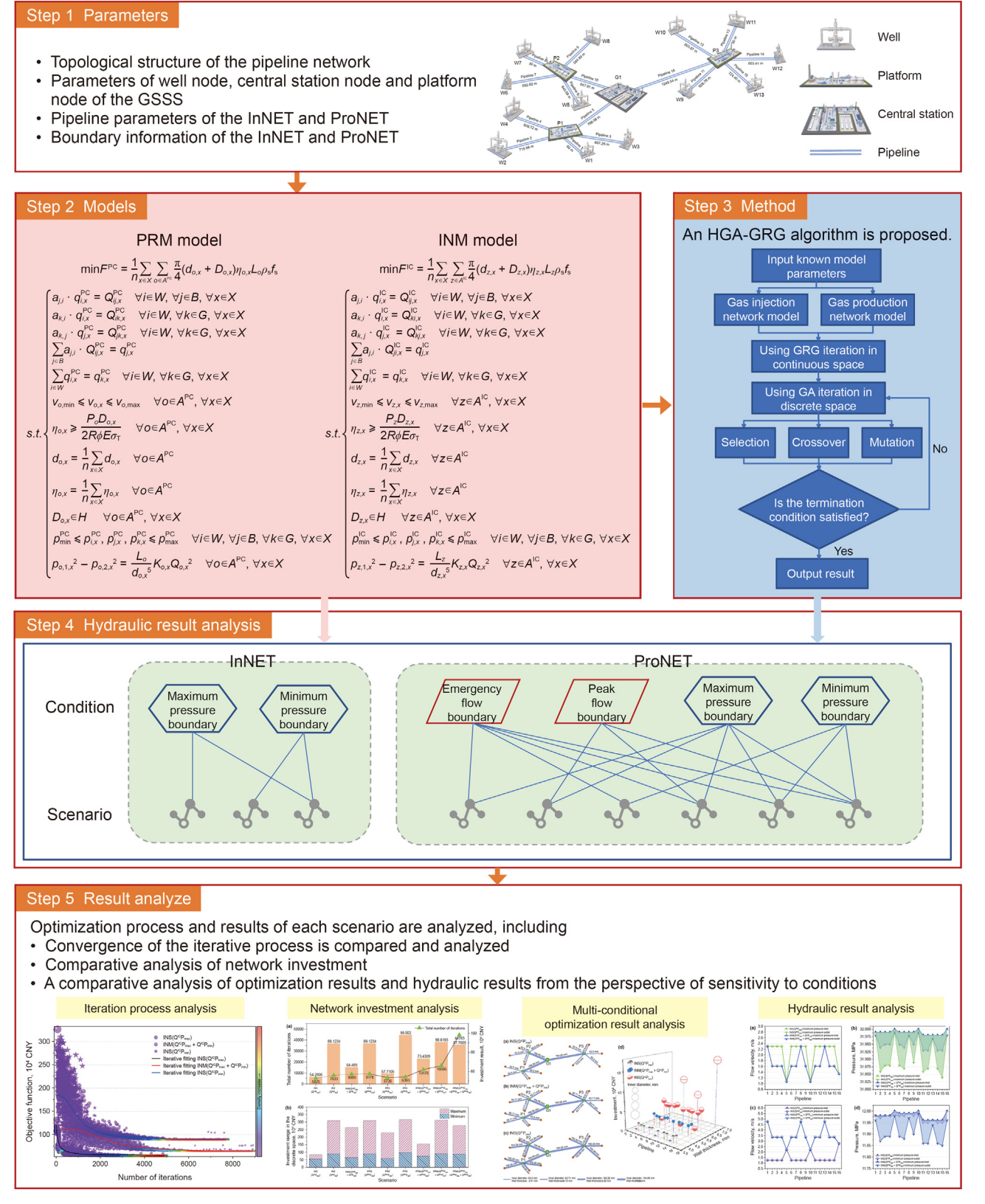


Fig. 5. Optimization framework.

transforming them into unconstrained ones. While effective for many applications, GRG does not always ensure the discovery of global optima.

Combining the strengths of GRG and GA, this paper develops an HGA-GRG algorithm, and its solution process is shown in Fig. 6. This

algorithm integrates solutions in both continuous and discrete spaces, applying GRG for continuous space optimization and adjusting feasible regions for discrete decision variables based on continuous optimization outcomes. This process uses continuous optimization results as the initial population for iterative

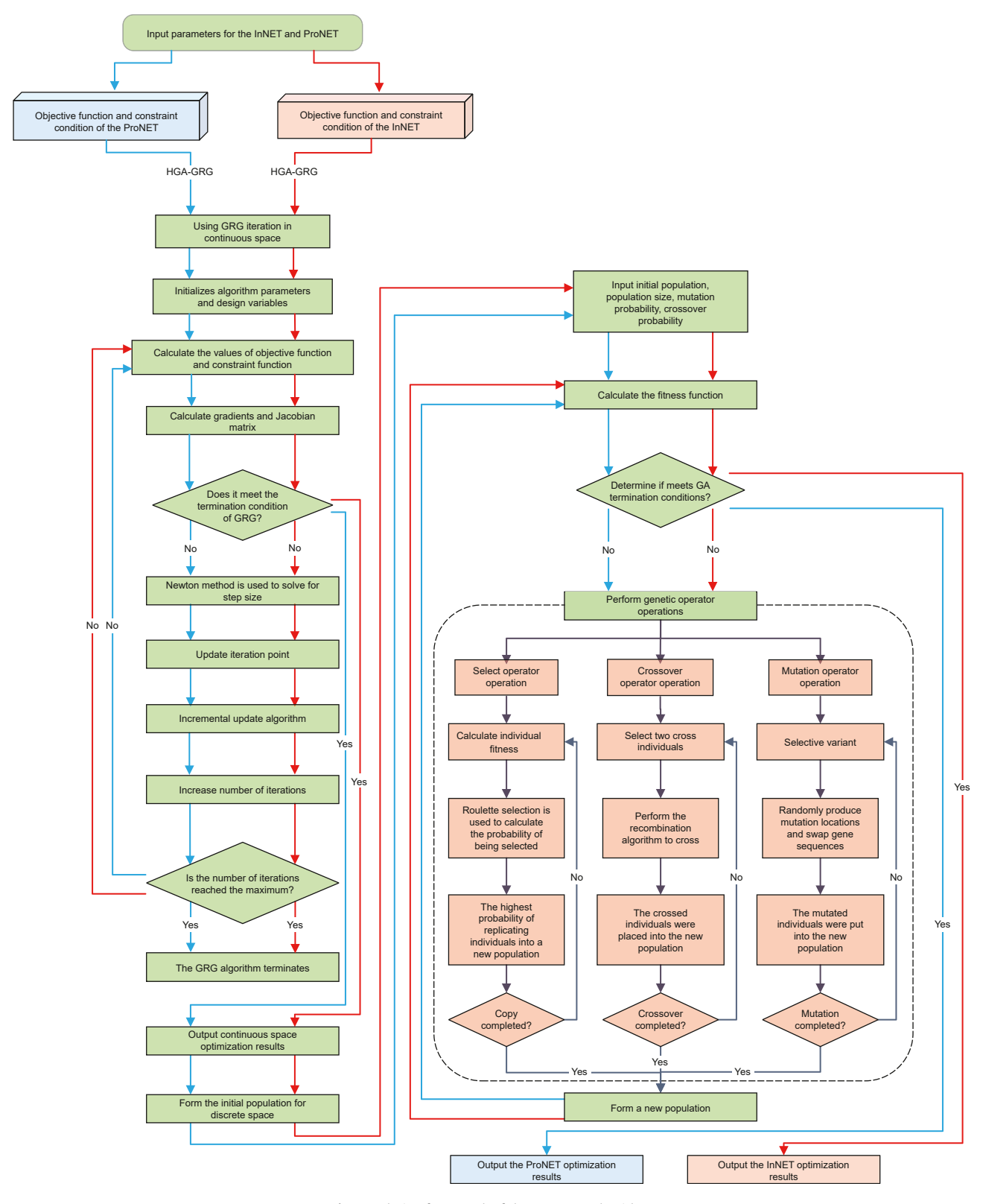


Fig. 6. Solution framework of the HGA-GRG algorithm.

optimization in discrete space, followed by further optimization using the genetic algorithm. The algorithm's steps include:

- (1) Define objective functions and constraints: represent the design parameter problem with an objective function and a set of equality and inequality constraints.
- (2) Initialize algorithm parameters and design variables: initialize algorithm parameters, define design variables as X_k , set iteration count k=0, and specify maximum iterations k_{\max} and precision ε . Initialize design variables.
- (3) Calculate the values for objective and constraint functions: substitute X_k into the objective function and constraint function to calculate the corresponding function value $F(X_k)$ and constraint function value $g(X_k)$.
- (4) Calculate gradients and Jacobian matrix: calculate the gradient h_k of the objective function and constraint function values with respect to the design variable X_k , as well as the Jacobian matrix J_k .
- (5) Compute the generalized gradient vector: The GRG algorithm employs a technique known as the reduced gradient to calculate gradients within a numerical error margin, accelerating optimization. The generalized gradient vector G_k can be calculated as shown in Eq. (39).

$$G_k = h_k - J_k^T \cdot \left(J_k \cdot J_k^T\right)^{-1} \cdot \left(J_k \cdot h_k - g(X_k)\right) \tag{39}$$

- (6) Check termination constraints: terminate the algorithm and output X_k as the optimal solution if $||G_k|| < \varepsilon$ are met, and proceed to step (12); otherwise, proceed to the next step.
- (7) Solve for step size α_k : use Newton's method to find the step size α_k that minimizes $F(X_k + \alpha_k G_k)$.
- (8) Update iteration point: calculate the next iteration point $X_{k+1} = X_k + \alpha_k G_k$.
- (9) Incremental update algorithm: update the Jacobian matrix and generalized gradient vector as shown in Eq. (40).

$$J_{k+1} = J_k + \Delta J_k G_{k+1} = G_k + \Delta G_k$$
 (40)

- (10) Increase number of iterations: increment the iteration count k = k + 1.
- (11) Check if the number of iterations has reached the maximum: If $k < k_{\text{max}}$, return to step (3); otherwise, note that GRG has not found an optimal solution in continuous space.
- (12) Output continuous space optimization results. Form the initial population for discrete space. Input the initial population and other algorithm parameters.
- (13) Evaluate fitness of each individual in the initial population, calculating corresponding objective function values.
- (14) Determine if the highest fitness individual meets GA termination conditions. If it does, proceed to step (17) to output the design variables. Otherwise, proceed to the next step.
- (15) Perform genetic operator operations:
 - Select operator operation: select individuals with higher fitness to serve as parents for the next generation. The bestpreserved selection method is used to calculate the probability of being selected.
 - Crossover operator operation: based on the characteristics of decision variables, floating-point encoding is adopted for the recombination algorithm to cross individual genes.
 - 3) Mutation operator operation: real-value mutation method based on order mutation is used for the mutation operation. This method randomly generates two mutation positions and then swaps the genes at these two positions.
- (16) Form a new population and return to step (13).
- (17) Output the optimized discrete pipeline design parameters.

5. Case description

5.1. Basic data

UNGSs are currently in rapid development, with the scale of operational UNGS being relatively small. To facilitate the management of injection and production operations, many current UNGS adopt a star-shaped topology design, such as China's Hutubi Gas Storage. A case study is established as shown in Fig. 7. According to Table 1, the injection flow for well nodes is defined as 11.5×10^4 m³/d, the peak production flow is 15.4×10^4 m³/d, and the emergency production flow is 60×10^4 m³/d. The economic flow velocity range for both InNET and ProNET is between 1 and 15 m/s.

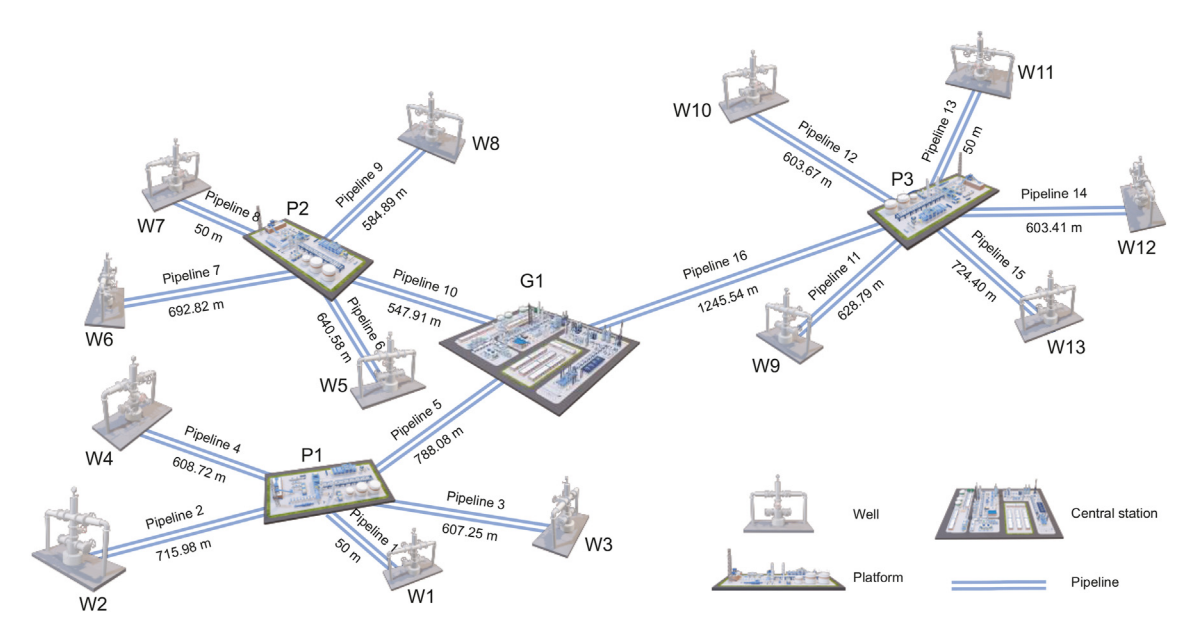


Fig. 7. Topology diagram of the network.

Table 1Parameters of each node in the InNET and ProNET.

No.	Parameter type		Value
1	Central station parameters	Number of central stations	1
2		Maximum pressure, MPa	32
3		Minimum pressure, MPa	12
4		Outlet temperature, °C	50
5		Injection capacity of GSSS, 10 ⁴ m ³ /d	149.5
6		Peak production capacity of GSSS, 10 ⁴ m ³ /d	200.2
7		Emergency production capacity of GSSS, 10 ⁴ m ³ /d	780
8	Platform parameters	Number of platforms	3
9		Maximum pressure, MPa	32
10		Minimum pressure, MPa	12
11		Maximum flow, 10^4 m ³ /d	300
12	Injection and production well parameters	Number of wells	13
13		Maximum pressure per well, MPa	32
14		Minimum pressure per well, MPa	12
15		Production temperature per well, °C	75
16		Injection capacity per well, 10 ⁴ m ³ /d	11.5
17		Peak production capacity per well, 10 ⁴ m ³ /d	15.4
18		Emergency production capacity per well, 10 ⁴ m ³ /d	60

Table 2 Components of natural gas.

No.	Component	Mole fraction, %
1	H ₂	2.6
2	N_2	1.41
3	CO_2	0.48
4	H ₂ S	0.01
5	COS	0.03
6	H ₂ O	0.04
7	CH ₄	92.51
8	C_2H_6	2.54
9	C₃H ₈	0.27
10	CH ₃ SH	0.06
11	C ₂ H ₅ SH	0.02
12	He	0.03

The natural gas transported in this case study has a complex composition. The components of the natural gas are shown in Table 2. It's important to note that temperature and pressure significantly affect the physical properties of natural gas. Specifically, under different injection and production temperatures (50 and 75 °C) and pressure boundaries (32 and 12 MPa), the physical properties of natural gas are as shown in Table 3.

5.2. Scenario setting

To verify the models and algorithms proposed in this paper, three scenarios for the InNET and six scenarios for the ProNET are set up. In the InNET, as gas is injected into UNGS, the well pressure gradually transitions from the minimum pressure to the maximum pressure. Therefore, this paper employs the INS model to set up two scenarios: $INS(Q^{IC}P_{max}) \ \, \text{and} \ \, INS(Q^{IC}P_{min}), \ \, \text{where the scenario using the maximum pressure boundary is }INS(Q^{IC}P_{max}), \, \text{and the scenario using}$

the minimum pressure boundary is $INS(Q^{IC}P_{min})$. Additionally, the INM model is used to set up the scenario $INM(Q^{IC}P_{max}+Q^{IC}P_{min})$, which simultaneously couples both the maximum and minimum pressure boundaries. The conditions for these three scenarios are shown in Fig. 8.

This paper considers emergency production boundary and peak production boundary for the different flow, and maximum and minimum pressure boundaries. The six scenarios for the ProNET are shown in Fig. 9. Among them, PRS(QPPCPmax), PRS(QEPCPmax), and PRS(QEPCPmin) utilize the PRS model, operating under a single condition. The scenario PRM(QEPCPmax + QPPCPmax) in the maximum pressure couples the well flow boundary, being capable of satisfying both the emergency production boundary at maximum pressure and the peak production boundary at maximum pressure. Similarly, the scenario PRM(QEPCPmax + QEPCPmin) couples the well pressure boundary; and PRM(QEPCPmax + QPPCPmax + QEPCPmin) simultaneously couples three conditions.

To analyze the applicability of the optimization results under different conditions, this paper simulates and analyzes the hydraulic characteristics of the optimization model results. For instance, for ${\sf INS}(Q^{\sf IC}P_{\sf min})$, optimized under the minimum pressure boundary, its performance under the maximum pressure boundary needs to be comparatively studied. Therefore, this paper employs simulation software to simulate the optimized results under other conditions, as shown in Table 4.

6. Result and discussion

6.1. Iteration process analysis

6.1.1. Algorithm comparison

To validate the characteristics of the HGA-GRG algorithm proposed in this paper, both the HGA-GRG and traditional GA were

Table 3 Physical properties of natural gas.

No.	. Physical properties	Injection condition (32 MPa, 50	Injection condition (12 MPa, 50	Production condition (32 MPa, 75	Production condition (12 MPa, 75
		°C)	°C)	°C)	°C)
1	Average molecular weight	13.8412	13.8412	13.8412	13.8412
2	Specific heat, kJ/kg·°C	47.6107	42.9215	46.8315	42.4744
3	Kinematic viscosity, cSt	0.1279	0.2149	0.1365	0.2448
4	Viscosity, cP	0.0213	0.0144	0.0207	0.0148
5	Thermal conductivity, W/	0.0873	0.0617	0.0871	0.0652
	$m \cdot K$				

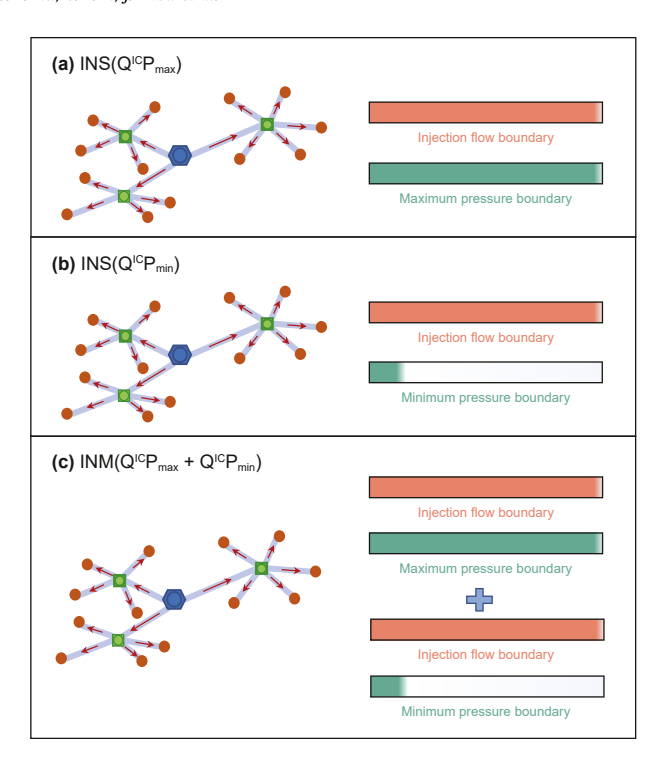


Fig. 8. Scenario diagrams for the InNET: (a) INS($Q^{IC}P_{max}$); (b) INS($Q^{IC}P_{min}$); (c) INM($Q^{IC}P_{max} + Q^{IC}P_{min}$).

used to optimize INS($Q^{IC}P_{max}$), with the iterative processes shown in Fig. 10. The HGA-GRG converged to 54.2806 \times 10⁴ CNY after only 5025 iterations, while the GA required 37,992 iterations to converge to 57.9451 \times 10⁴ CNY. The GRG can extend linear constraint optimization to nonlinear scenarios, effectively handling constraint

optimization and thus compensating for the shortcomings of GA. As shown in Fig. 10, the HGA-GRG combines the global search capability of GA with the fine-grained local search capability of GRG, enhancing the algorithm's convergence speed and accuracy. This algorithm maintains lower error fluctuations over extended iterations, resulting in more stable optimization performance.

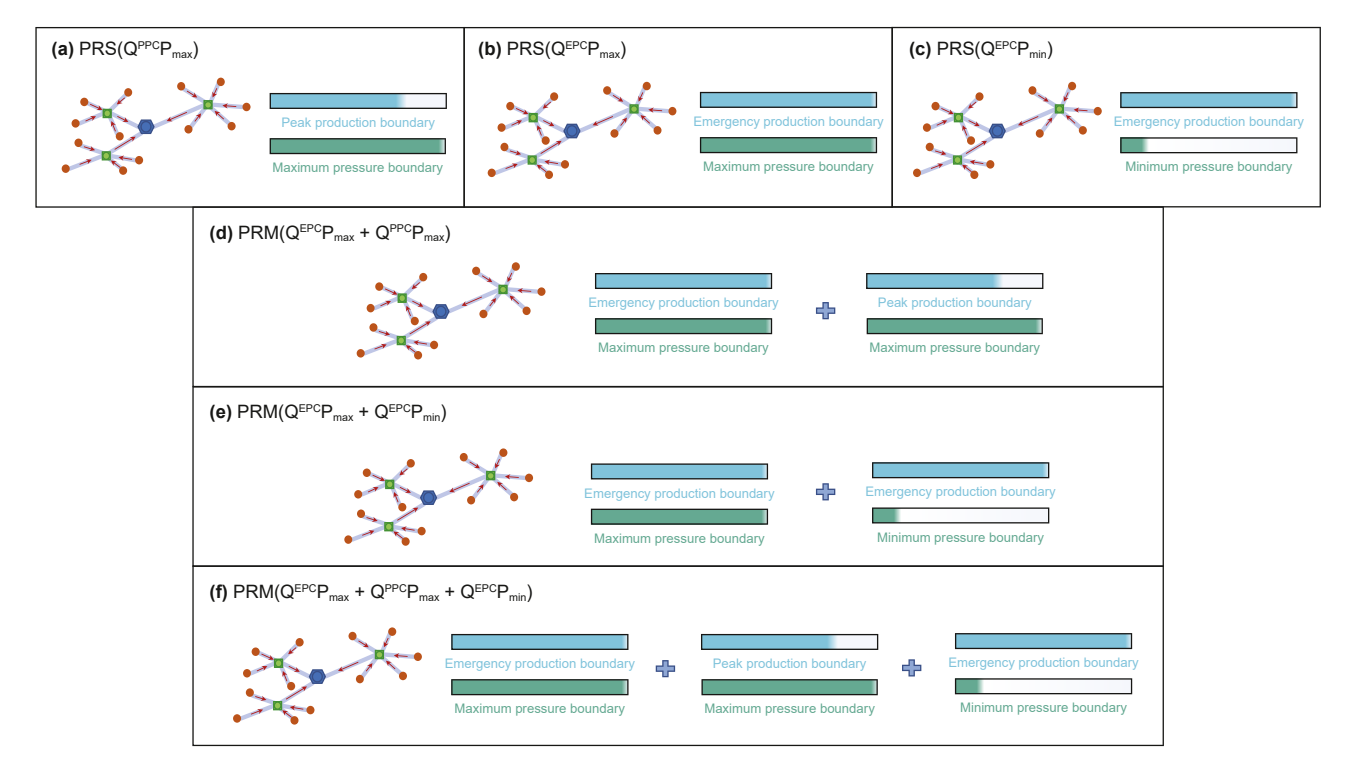
6.1.2. Convergence analysis of the InNET

To investigate the iterative convergence differences under various conditions within the InNET, the HGA-GRG algorithm was employed to optimize scenarios INS(QICPmax), INS(QICPmin), and $INM(Q^{IC}P_{max} + Q^{IC}P_{min})$. The iteration process is depicted in Fig. 11, showing the scatter data distribution and fitting curves under three scenarios. As the iterations increase, the fluctuation range of the objective function gradually decreases, the distribution density of data points increases, and they tend to concentrate along the fitting curves. INS(QICP_{max}) is the first to converge, with an initially steep fitting curve that gradually stabilizes. Next is INS(Q^{IC}P_{min}), which converges more slowly compared to the former. Finally, INM(Q^{IC}P_{max} + O^{IC}P_{min}) converges. Overall, the trend of the iteration fitting curves for the three scenarios indicates that INS(Q^{IC}P_{max}) converges more quickly and requires the fewest iterations, resulting in the smallest convergence result. $INM(Q^{IC}P_{max} + Q^{IC}P_{min})$ starts to show convergence after 5800 iterations due to considering both minimum and maximum pressure boundaries, leading to the longest number of iterations.

6.1.3. Convergence analysis of the ProNET

To explore the iterative convergence differences under various conditions within the ProNET, the algorithm was utilized to optimize six scenarios, as shown in Fig. 12.

In Fig. 12(a), PRS(Q^{PPC}P_{max}) has the fewest iterations and yields the lowest network cost. However, the optimized pipeline diameter parameters may not satisfy the emergency production boundaries.



 $\begin{aligned} \textbf{Fig. 9.} & \text{ Scenario diagrams for the ProNET: } \textbf{(a)} & \text{PRS}(Q^{PPC}P_{max}); \textbf{(b)} & \text{PRS}(Q^{EPC}P_{max}); \textbf{(c)} & \text{PRS}(Q^{EPC}P_{min}); \textbf{(d)} & \text{PRM}(Q^{EPC}P_{max} + Q^{PPC}P_{max}); \textbf{(e)} & \text{PRM}(Q^{EPC}P_{max} + Q^{EPC}P_{min}); \textbf{(f)} & \text{PRM}(Q^{EPC}P_{max} + Q^{EPC}P_{min}); \textbf{(f)} & \text{PRM}(Q^{EPC}P_{max} + Q^{EPC}P_{min}); \textbf{(g)} & \text{PRM}(Q^{EPC}P_{min}); \textbf{(g)} & \text{PRM}(Q^{EPC}P_{max} + Q^{EPC}P_{min}); \textbf{(g)} & \text{PRM}(Q^{EPC}P_{min}); \textbf{(g)} & \text{PRM}(Q^{EPC}P$

Table 4Simulation scenario settings for the InNET and ProNET.

Network	Simulation naming	Optimization condition	Simulation condition
InNET	SIM _{INS-HP}	$INS(Q^{IC}P_{min})$	Maximum pressure condition
	SIM _{INS-LP}	$INS(Q^{IC}P_{max})$	Minimum pressure condition
ProNET	$SIM_{PRS-EPC}$	$PRS(Q^{PPC}P_{max})$	Emergency production condition
	$SIM_{PRS-PPC}$	$PRS(Q^{EPC}P_{max})$	Peak production condition
	SIM_{PRS-HP}	$PRS(Q^{EPC}P_{min})$	Maximum pressure condition
	SIM_{PRS-LP}	$PRS(Q^{EPC}P_{max})$	Minimum pressure condition
	$SIM_{PRM-(PPC + LP)}$	$PRM(Q^{EPC}P_{max} + Q^{EPC}P_{min})$	Peak production condition + Minimum pressure condition
	$SIM_{PRM-(PPC + HP)}$	$PRM(Q^{EPC}P_{max} + Q^{EPC}P_{min})$	Peak production condition + Maximum pressure condition
	$SIM_{PRM-(LP + EPC)}$	$PRM(Q^{EPC}P_{max} + Q^{PPC}P_{max})$	Minimum pressure condition + Emergency production condition
	$SIM_{PRM-(LP + PRC)}$	$PRM(Q^{EPC}P_{max} + Q^{PPC}P_{max})$	$Minimum\ pressure\ condition + Peak\ production\ condition$

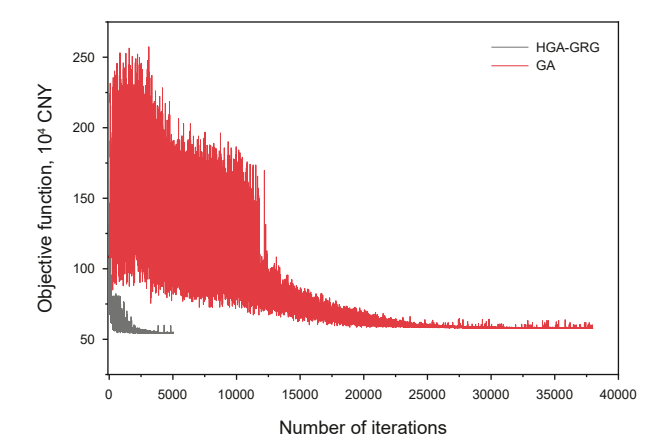


Fig. 10. Iterative comparison of HGA-GRG and GA algorithms.

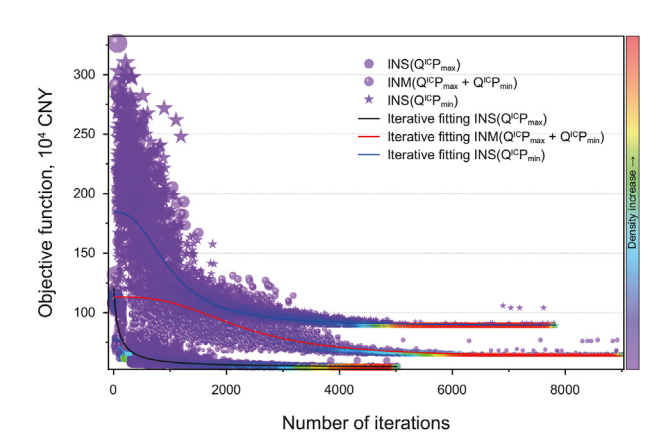
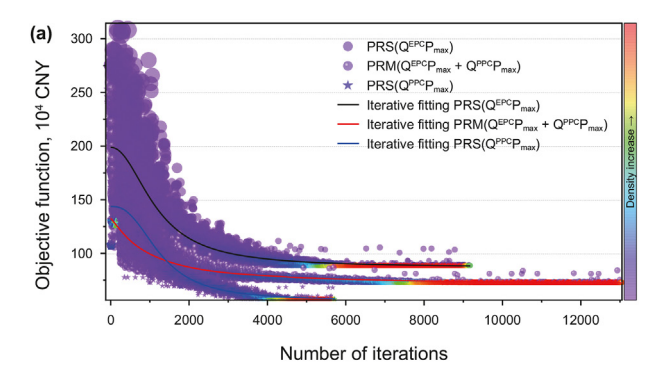
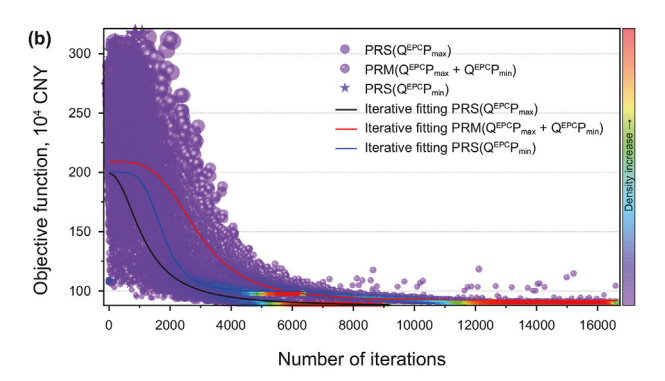


Fig. 11. Comparison of iteration processes in the InNET.

PRM(Q^{EPC}P_{max} + Q^{PPC}P_{max}), which considers both emergency and peak production boundaries during its iteration process, shows a relatively slow convergence speed compared to the other two scenarios. It begins to gradually converge around 7500 iterations, with its final convergence cost lying between those of PRS(Q^{PPC}P_{max}) and PRS(Q^{EPC}P_{max}). In Fig. 12(b), the three scenarios exhibit a rapid convergence speed in the initial 4000 iterations. PRS(Q^{EPC}P_{min}) is the first to begin converging, followed by PRM(Q^{EPC}P_{max} + Q^{EPC}P_{min}), which starts showing convergence around 11700 iterations. In Fig. 12(c), since PRM(Q^{EPC}P_{max} + Q^{PPC}P_{max} + Q^{EPC}P_{min}) simultaneously couples three conditions, satisfying the single-condition scenarios of PRS(Q^{EPC}P_{max}), PRS(Q^{PPC}P_{max}), and PRS(Q^{EPC}P_{min}) compared to PRM(Q^{EPC}P_{max} + Q^{PPC}P_{max}) and PRM(Q^{EPC}P_{max} + Q^{EPC}P_{min}).





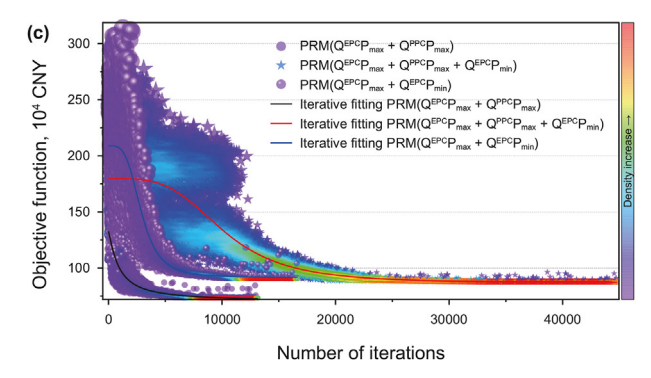


Fig. 12. Comparison of iteration processes in the ProNET: (**a**) flow variation conditions; (**b**) pressure variation conditions; (**c**) flow and pressure variation conditions.

6.2. Network investment analysis

Fig. 13 shows the iteration results for each scenario. During the iteration process, after obtaining continuous optimal solutions, the algorithm narrows down the range of solutions in the discrete space and continues to solve using the GA within the constraints. Since the

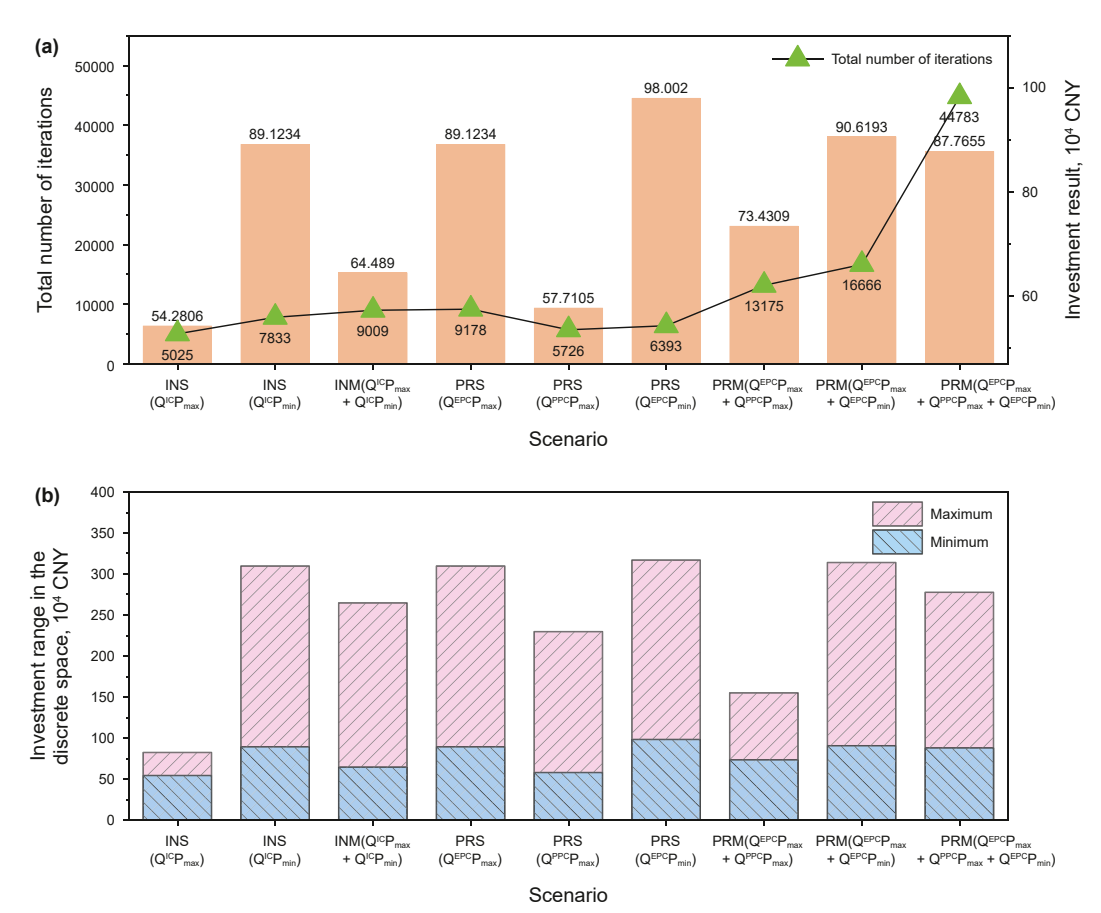


Fig. 13. Iteration results for each scenario: (a) total number of iterations and investment results; (b) investment range in the discrete space.

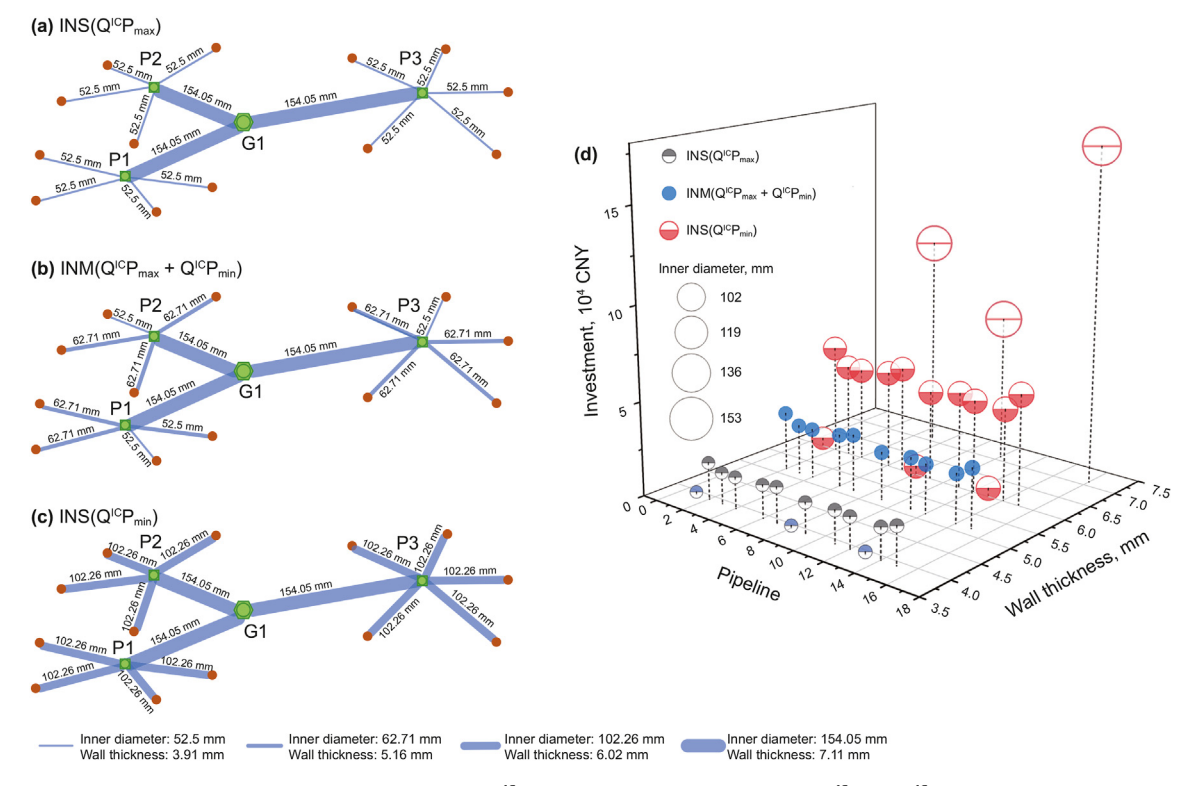


Fig. 14. Optimization results for the InNET: (a) diameter parameters for INS(Q^{IC}P_{max}); (b) diameter parameters for INM(Q^{IC}P_{min}); (c) diameter parameters for INS(Q^{IC}P_{min}); (d) investment.

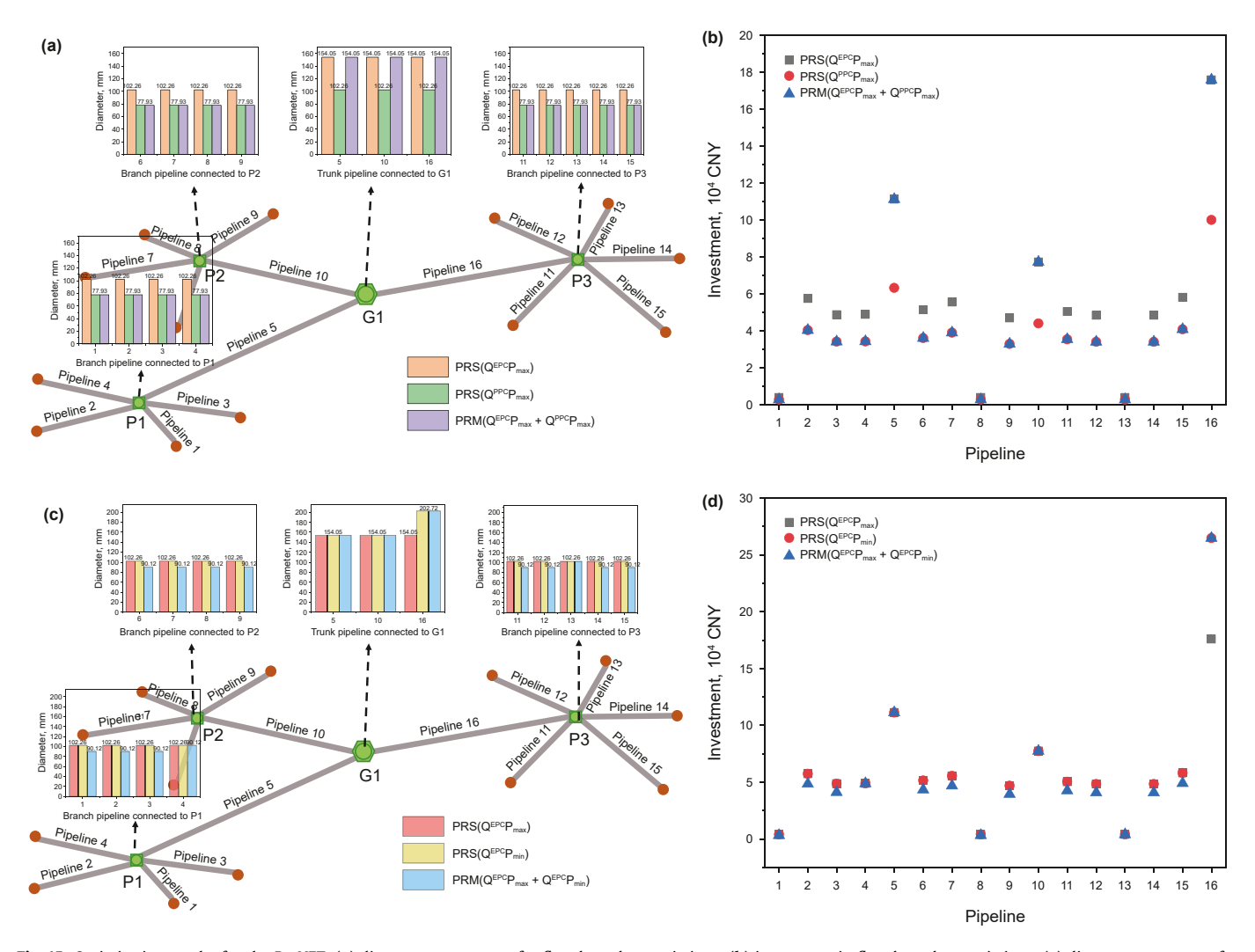


Fig. 15. Optimization results for the ProNET: (a) diameters parameters for flow boundary variations; (b) investment in flow boundary variations; (c) diameter parameters for pressure boundary variations; (d) investment in pressure boundary variations.

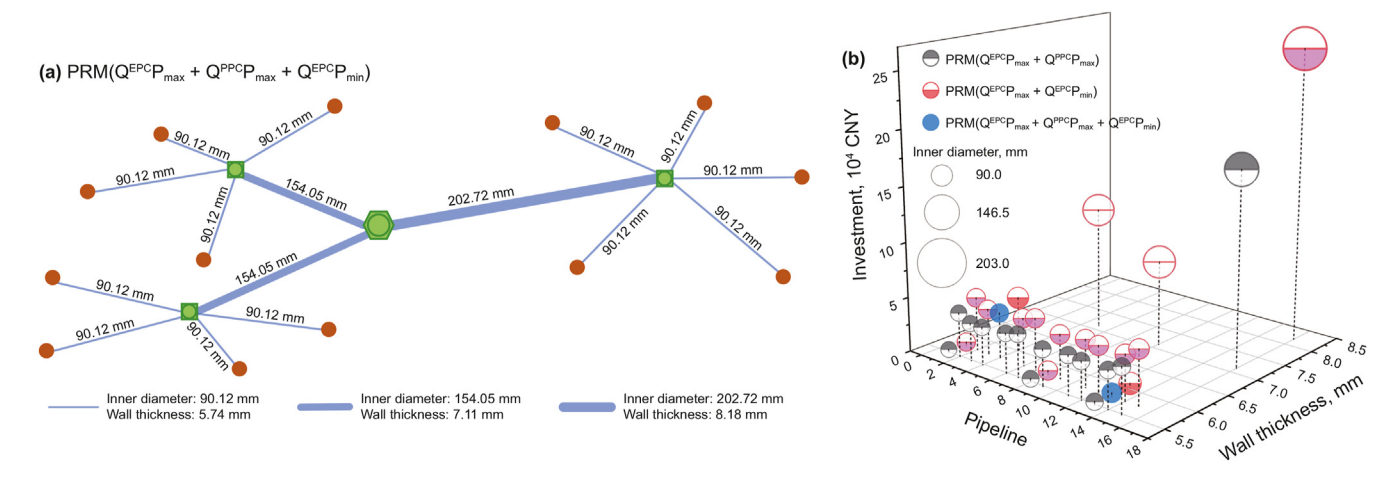


Fig. 16. Optimization results for the ProNET: (a) diameter parameters for PRM $(Q^{EPC}P_{max} + Q^{PPC}P_{max} + Q^{EPC}P_{min});$ (b) investment.

number of iterations in the continuous space is significantly small compared to the total number of iterations and the investment range is much smaller than in the discrete space, the investment range of the objective function in this study mainly targets the discrete space.

In the InNET, the final investment for INM($Q^{IC}P_{max}+Q^{IC}P_{min}$) is 64.4890 \times 10⁴ CNY, which lies between the other two scenarios. In the discrete space, INS($Q^{IC}P_{max}$) has the smallest investment range, while INM($Q^{IC}P_{max}+Q^{IC}P_{min}$) and INS($Q^{IC}P_{min}$) have larger

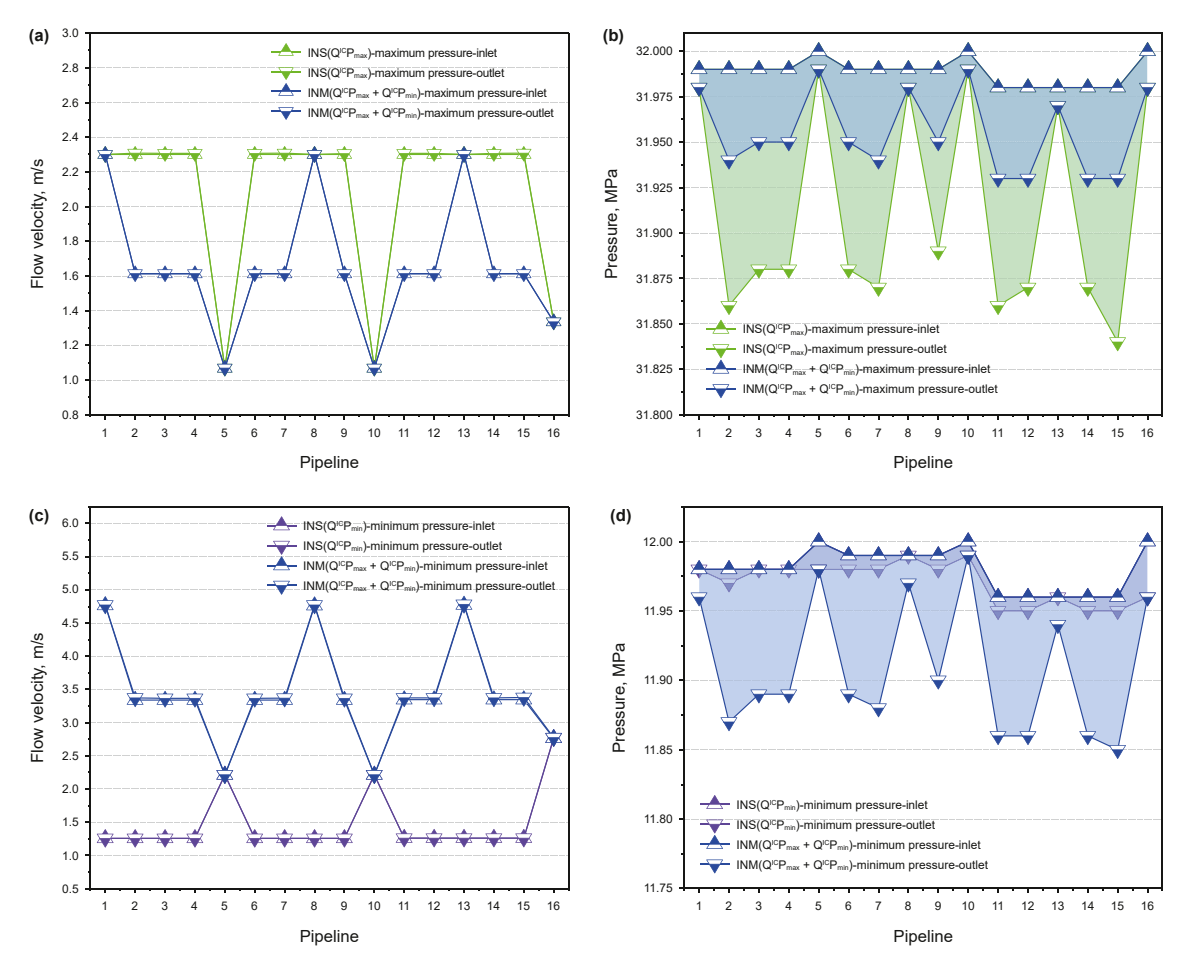


Fig. 17. Velocity and pressure distribution in InNET. (a) velocities under maximum pressure boundary; (b) pressures under maximum pressure boundary; (c) velocities under minimum pressure boundary; (d) pressures under minimum pressure boundary.

investment ranges during the iteration process.

In the ProNET, for the flow boundary, since PRS(Q^{EPC}P_{max}) requires larger pipeline diameters and wall thicknesses due to higher well node flows, it results in a higher investment in the discrete space. Conversely, PRS(Q^{PPC}P_{max}) has a lower investment. PRM(Q^{EPC}P_{max} + Q^{PPC}P_{max}) shows a smaller investment range of the objective function value in the discrete space compared to the first two scenarios, thus stabilizing more easily during iterations. For the pressure boundary, the investment of PRM(Q^{EPC}P_{max} + Q^{EPC}P_{min}) lies between the investment of PRS(Q^{EPC}P_{max}) and PRS(Q^{EPC}P_{min}), but its optimization results are more applicable. PRM(Q^{EPC}P_{max} + Q^{PPC}P_{max} + Q^{EPC}P_{min}) achieves a investment that is 2.8538 \times 10⁴ CNY lower than PRM(Q^{EPC}P_{max} + Q^{EPC}P_{min}) and 14.3346 \times 10⁴ CNY higher than PRM(Q^{EPC}P_{max} + Q^{EPC}P_{max}). However, from the perspectives of cost-effectiveness and applicability, its optimized results are more attractive.

6.3. Multi-condition optimization result analysis

6.3.1. Pressure boundary analysis for the InNET

The optimization results and pipeline investment under three pressure conditions of the InNET are shown in Fig. 14. The trunk pipelines optimized in the three scenarios have the same diameter and wall thickness, among which pipeline 16 has the longest transportation distance, hence the largest investment at 17.5855 \times 10⁴ CNY in Fig. 14(b). It is found that the pipeline diameter parameters optimized by INS(Q^{IC}P_{min}) are relatively larger, followed

by $INM(Q^{IC}P_{max} + Q^{IC}P_{min})$, confirming the observation that the pipeline investment optimized by $INS(Q^{IC}P_{min})$ are generally higher as shown in Fig. 13(b).

6.3.2. Flow boundary analysis for the ProNET

The optimization results and pipeline investment under flow boundaries of the ProNET are shown in Fig. 15. As seen in Fig. 15(a), three scenarios optimized two different sets of pipeline parameters. Since trunk pipelines 5, 10, and 16 transport larger flows, larger pipeline parameters were optimized. The pipeline parameters optimized by PRS(QEPCPmax) are larger than those by PRS(QPPCPmax), while the parameters obtained by PRM(QEPCPmax + QPPCPmax) match the trunk pipeline parameters of PRS(QEPCPmax), leading to identical corresponding pipeline investment in Fig. 15(b). The minimum pipeline investment in all three scenarios are for pipelines 1, 8, and 13, which is attributed to the lengths of the pipelines.

6.3.3. Pressure boundary analysis for the ProNET

The optimization results and pipeline investment under pressure conditions of the ProNET are shown in Fig. 15. From Fig. 15(c), it can be seen that $PRM(Q^{EPC}P_{max} + Q^{EPC}P_{min})$ yielded pipeline parameters with greater diversity. Compared to $PRS(Q^{EPC}P_{max})$, the pipeline parameters optimized by $PRS(Q^{EPC}P_{min})$ only differed for pipeline 16, resulting in identical investment for pipelines 1 to 15 between the two scenarios in Fig. 15(d). The larger parameters for pipeline 16 in $PRS(Q^{EPC}P_{min})$ ensure the network operates normally

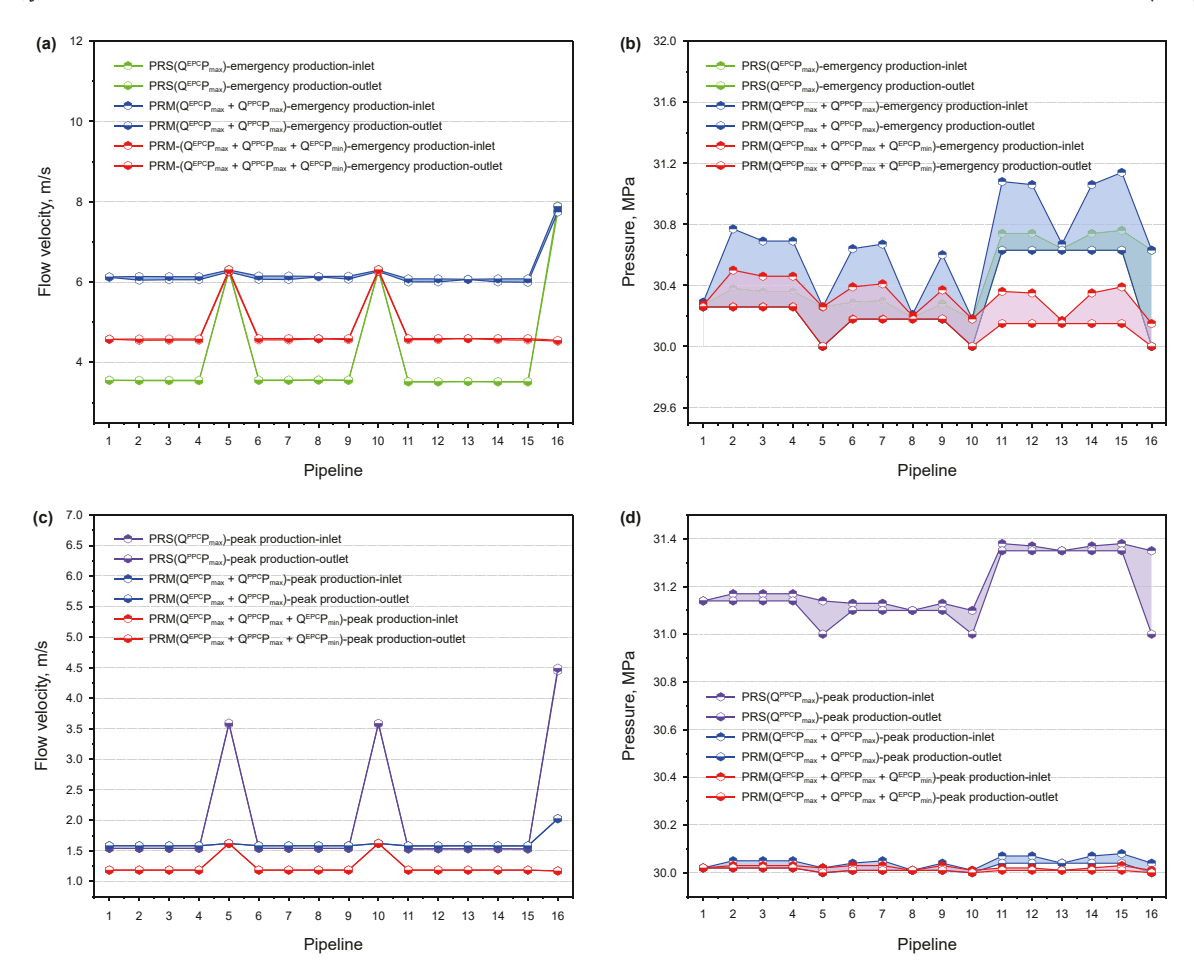


Fig. 18. Velocity and pressure distribution in ProNET. (a) velocities under emergency production boundaries; (b) pressures under emergency production boundary; (c) velocities under peak production boundary; (d) pressures under peak production boundary.

under emergency peak conditions and the lowest pressure conditions. In PRM(Q^{EPC}P_{max} + Q^{EPC}P_{min}), the shortest branch pipelines 1 and 8 have the smallest optimized wall thicknesses and diameters, hence having the lowest investment of 0.339 \times 10 4 CNY.

6.3.4. Pressure and flow boundary analysis for the ProNET

The pipeline types and investment optimized by PRM(QEPCP_{max} $+ Q^{PPC}P_{max} + Q^{EPC}P_{min}$) are shown in Fig. 16, with a comparison of scenarios using the PRM model in Fig. 16(b). Fig. 16(a) reveals that the network optimized by $PRM(Q^{EPC}P_{max} + Q^{PPC}P_{max} + Q^{EPC}P_{min})$ used three different types of pipelines. Compared to all previously discussed optimization results for the ProNET, the trunk pipeline 16 optimized by $PRM(Q^{EPC}P_{max} + Q^{PPC}P_{max} + Q^{EPC}P_{min})$ had the largest parameters, and the parameters for trunk pipelines 5 and 10 showed a high consistency with those from all scenarios. The branch pipeline parameters optimized by PRM(QEPCPmax + $Q^{PPC}P_{max} + Q^{EPC}P_{min}$) were the larger ones among PRM($Q^{EPC}P_{max} + Q^{PPC}P_{max}$) and PRM($Q^{EPC}P_{max} + Q^{EPC}P_{min}$), with a wall thickness of 5.74 mm and an inner diameter of 90.12 mm. Therefore, its optimization results can ensure safe operation of each pipeline under multiple conditions. Moreover, since the branch pipeline parameters optimized by $PRM(Q^{EPC}P_{max} + Q^{PPC}P_{max} + Q^{EPC}P_{min})$ and $PRM(Q^{EPC}P_{max} + Q^{EPC}P_{min})$ were mostly the same, these pipelines had the same investment in Fig. 16(b), making the total investment of these two scenarios similar.

6.4. Hydraulic result analysis

6.4.1. Hydraulic analysis of the InNET

Hydraulic analysis was performed on the optimization results for $INS(Q^{IC}P_{max})$, $INS(Q^{IC}P_{min})$, and $INM(Q^{IC}P_{max} + Q^{IC}P_{min})$, as shown in Fig. 17. Since the trunk pipeline diameters optimized in the three scenarios were the same, the flow velocities of pipelines 5, 10, and 16 under the constraint conditions were the same in Fig. 17(a) and (c). Similarly, the branch pipeline parameters optimized by $INS(Q^{IC}P_{max})$ and $INM(Q^{IC}P_{max} + Q^{IC}P_{min})$ were the same, so in Fig. 17(a), the inlet and outlet flow velocities for pipelines 1, 8, and 13 were identical. In Fig. 17(b) and (d), the three scenarios showed the same pressure distribution trend under maximum and minimum pressures. Since $INS(Q^{IC}P_{max})$ optimized smaller branch pipe diameters with higher velocities, it resulted in a larger pressure drop compared to the others. The velocity and pressure of each pipeline were within the constraint range, effectively verifying the correctness of the model and algorithm.

6.4.2. Hydraulic analysis of the ProNET

For the different flow boundaries, hydraulic analysis was conducted on the optimization results for $PRS(Q^{EPC}P_{max})$, $PRS(Q^{PPC}P_{max})$, $PRM(Q^{EPC}P_{max} + Q^{PPC}P_{max})$, and $PRM(Q^{EPC}P_{max} + Q^{PPC}P_{max} + Q^{EPC}P_{min})$, as depicted in Fig. 18. The velocity and pressure of each pipeline were within the constraint range. In Fig. 18(a), the average flow velocity was lower in the branch pipelines optimized by $PRS(Q^{EPC}P_{max})$ due to their larger diameters. Due to the higher flow

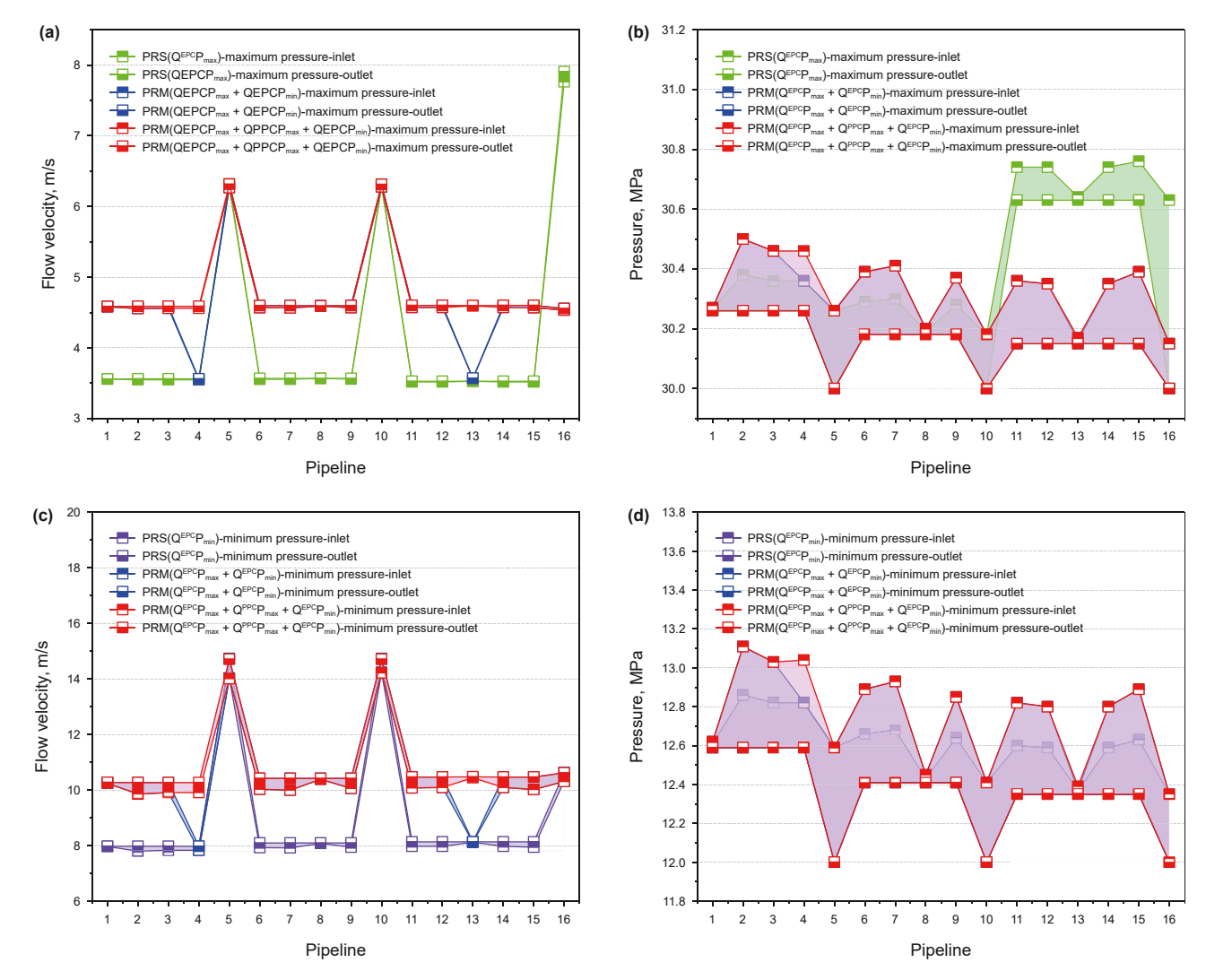


Fig. 19. Velocity and pressure distribution in ProNET. (a) velocities under maximum pressure boundary; (b) pressures under maximum pressure boundary; (c) velocities under minimum pressure boundary; (d) pressures under minimum pressure boundary.

rate of emergency production boundary, Fig. 18(b) shows larger pressure drops across the pipelines. In Fig. 18(c) and (d), since $PRS(Q^{PPC}P_{max})$ optimized smaller diameters for the trunk pipelines compared to the other two scenarios, the inlet and outlet velocities for pipelines 5, 10, and 16 were higher, resulting in larger pressure drops.

For the different pressure boundaries, hydraulic analysis was performed on the optimization results for $PRS(Q^{EPC}P_{max}),$ $PRS(Q^{EPC}P_{min}),$ $PRM(Q^{EPC}P_{max} + Q^{EPC}P_{min}),$ and $PRM(Q^{EPC}P_{max} + Q^{PPC}P_{max} + Q^{EPC}P_{min}),$ as shown in Fig. 19. The velocity distribution at the inlets and outlets of each scenario's pipelines in Fig. 19(a) and (c) was similar, with differences in pipeline velocities primarily caused by pipeline parameters. Comparing Fig. 19(b) and (d), the pressure distribution in the network had the same trend, with trunk pipelines experiencing lower pressures compared to branch lines due to differences in diameter and velocity. Additionally, the pipeline pressures in all four scenarios were within the constraint range, indicating safe operation.

6.4.3. Comparative analysis of simulations

The flow velocities and the extreme values of inlet and outlet pressures for each simulation scenario are shown in Fig. 20. From Fig. 20, it can be seen that simulations that cannot meet the constraints include SIM_{INS-HP} , SIM_{INS-LP} , $SIM_{PRS-EPC}$, $SIM_{PRS-PPC}$, $SIM_{PRS-PPC}$, $SIM_{PRM-(PPC + HP)}$, and $SIM_{PRM-(LP + EPC)}$.

In Fig. 20(a), the minimum inlet and outlet flow velocities for SIM_{INS-HP} are around 0.6 m/s, failing to meet the flow velocity constraints. This is because the pipeline diameters optimized by single condition model INS(Q^{IC}P_{min}) are relatively large, leading to lower simulated flow velocities in most pipelines. Meanwhile, the maximum inlet flow velocity and maximum inlet and outlet pressures simulated by SIMPRS-EPC exceed the upper constraint limit, as PRS(Q^{PPC}P_{max}) is optimized for peak production conditions with smaller pipeline diameters. Therefore, when transporting larger flows, the overall pipeline flow velocity and pressure rise, especially for trunk pipelines, making it easier to exceed flow velocity constraints. Similarly, the remaining simulation scenarios fail to meet the constraints for the same reasons of inapplicability of their pipeline parameters to the simulated conditions. Generally, a larger proportion of simulation scenarios fail to meet the constraints, indicating that the fewer conditions considered during the pipeline parameter design process, the more limited its applicability. Therefore, through simulation scenario analysis, the widely applicability of PRM(QEPCPmax + QPPCP_{max} + QEPCP_{min}) in this case study is further highlighted, indirectly reflecting the multi -condition coupled models'

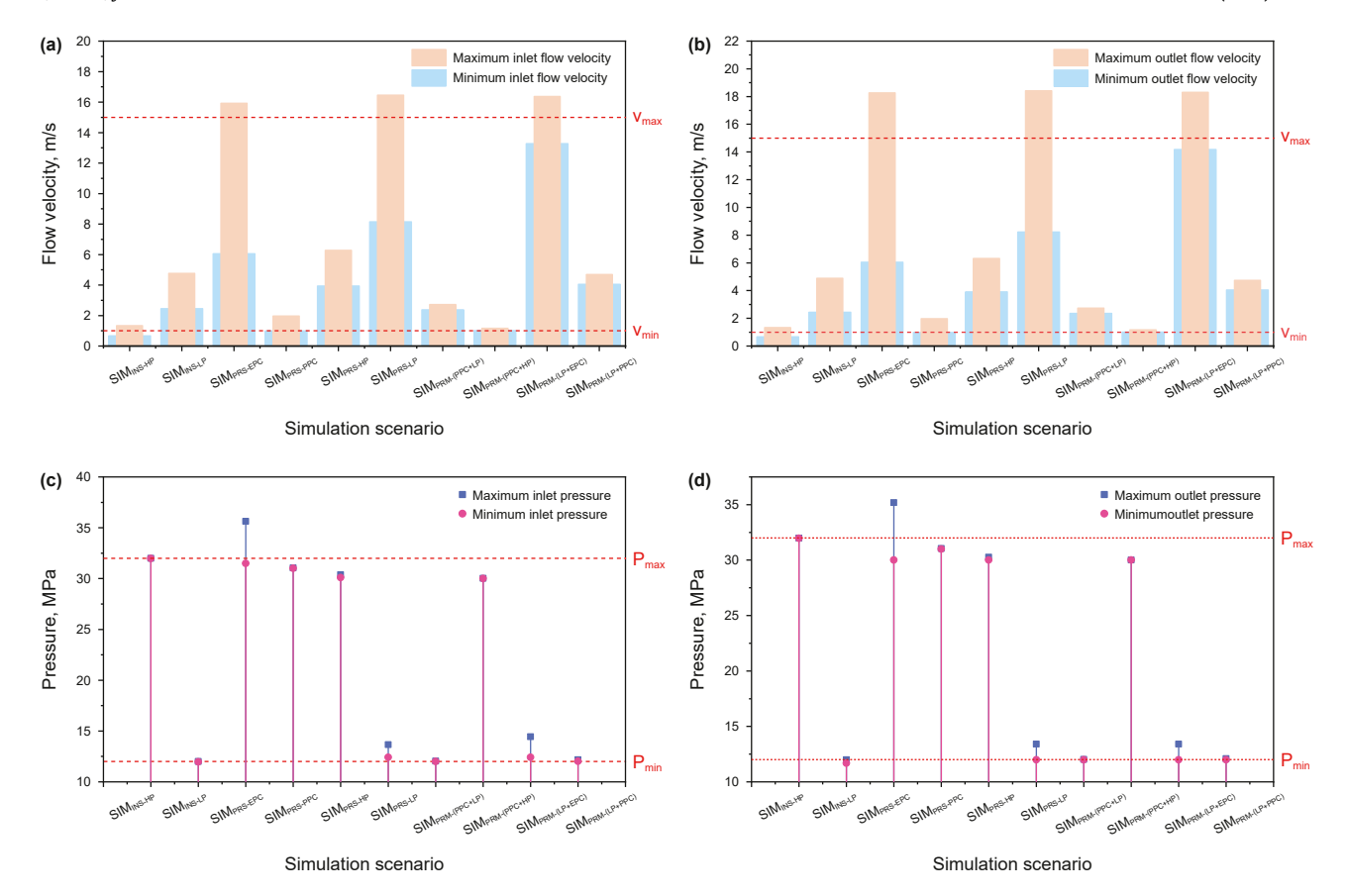


Fig. 20. Hydraulic results of simulation scenarios. (a) inlet flow velocities; (b) outlet flow velocities; (c) inlet pressures; (d) outlet pressures.

advantages of the INM model and PRM model proposed in this paper.

7. Conclusions

This paper constructs single condition models (INS model, PRS model) and multi-condition models (INM model and PRM model), aiming for the minimum pipeline investment. Furthermore, by integrating the GRG algorithm with GA, an HGA-GRG algorithm was proposed for the optimization of the models. Additionally, multiple scenarios were set up to study the impact of different conditions on the design results and the applicability of the models, leading to the following conclusions:

- (1) The HGA-GRG algorithm established solves in continuous space using the GRG algorithm. Based on the continuous optimization of pipeline parameters, the feasible domain of decision variables in discrete space is corrected, narrowing the discrete solution space. Discrete space iterative optimization is then performed using the continuous optimization results as the initial population. The iteration curve demonstrates stability throughout the iteration process.
- (2) A comparative analysis of the optimization results for INS(Q^{IC}P_{max}), INS(Q^{IC}P_{min}), and INM(Q^{IC}P_{max} + Q^{IC}P_{min}) under the InNET was conducted. The study shows that the cost of the InNET considering coupled pressure boundaries is 64.4890×10^4 CNY, and the optimization results can meet the constraints of both maximum and minimum pressures.

- (3) To clarify the impact of flow boundaries on pipeline parameters, a comparative analysis of the optimization results for PRS(Q^{EPC}P_{max}), PRS(Q^{PPC}P_{max}), and PRM(Q^{EPC}P_{max} + Q^{PPC}P_{max}) was conducted. Also, to reveal the impact of pressure boundaries on ProNET design parameters, a comparative analysis of the optimization results for PRS(Q^{EPC}P_{max}), PRS(Q^{EPC}P_{min}), and PRM(Q^{EPC}P_{max} + Q^{EPC}P_{min}) was performed. Lastly, the differences between PRM(Q^{EPC}P_{max} + Q^{PPC}P_{max} + Q^{EPC}P_{min}), PRM(Q^{EPC}P_{max} + Q^{PPC}P_{max}), and PRM(Q^{EPC}P_{max} + Q^{EPC}P_{min}) were analyzed. Results indicate that for the ProNET, the network cost is 87.7655 × 10⁴ CNY, proving to be more economical and applicable than other scenarios.
- (4) To explore the applicability of the optimization results simulation scenarios were set for simulating different flow and pressure boundaries. The results show that optimization results considering only a single condition or coupling two conditions are difficult to apply to other conditions. This confirms the widely applicability characteristic of scenarios considering coupled multiple conditions.
- (5) This paper primarily studies the impact of changes in well conditions during the injection and production processes on the optimization results of pipeline parameters. Future work could consider increasing the complexity of pipeline network design, selecting and investing in various surface facilities, studying the impact of different boundary characteristics on equipment operation, thereby obtaining the optimal pipeline investment and operating costs.

CRediT authorship contribution statement

Shi-Tao Liu: Writing — oiginal draft, writing — review & editing. **Cheng-Yu Li:** Writing — review & editing. **Jun Zhou:** Funding acquisition, Methodology. **Zi-Chen Li:** Software. **Zhan-Peng Ye:** Visualization. **Jing-Hong Peng:** Validation. **Yun-Xiang Zhao:** Data curation. **Guang-Chuan Liang:** Conceptualization.

Statement of data availability

All data, models, and code generated or used during the study appear in the submitted article.

Declaration of competing interests

The authors declare that there is no conflict of interests regarding the publication of this paper.

Acknowledgements

This work was funded by the National Natural Science Foundation of China, grant number 51704253 and 52474084.

Appendix A. Supplementary data

Supplementary data to this article can be found online at https://doi.org/10.1016/j.petsci.2025.04.009.

Nomenclature

Abbreviations

GSSS	Gas Storage Surface System
I NICT	Injustice Disable Nationals
InNET	Injection Pipeline Network
ProNET	Production Pipeline Network
UNGS	Underground Natural Gas Storage
IC	Injection Condition
PC	Production Condition
EPC	Emergency Production Condition
PPC	Peak Production Condition
INS model	Injection Single Condition Model
PRS model	Production Single Condition Model
INM model	Injection Multi-condition Coupled Model
PRM model	Production Multi-condition Coupled Model
GA	Genetic Algorithm
GRG	Generalized Reduced Gradient Algorithm
HGA-GRG	Hybrid Genetic Algorithm based on Generalized Reduced Gradient

Indexes and sets

A ^{IC}	Injection pipeline set, $z \in A^{IC} = \{1, 2,, N_z\}$
A^{PC}	Production pipeline set, $o \in A^{PC} = \{1, 2,, N_o\}$
В	Platform node set, $j \in B = \{1, 2,, N_j\}$
G	Central station node set, $k \in G = \{1, 2,, N_k\}$
Н	External diameter set, $D_z, D_o \in H = \{D_1, D_2,, D_n\}$
W	Well node set, $i \in W = \{1, 2,, N_i\}$
X	Condition set, $x \in X = \{1, 2,, N_x\}$

Parameters

$a_{j,i}$	Connection coefficient between platform node j and well node i ,
$a_{k,i}$	connected if $a_{j,i} = 1$, otherwise $a_{j,i} = 0$. Connection coefficient between central station node k and well
к,:	node <i>i</i> , connected if $a_{k,i} = 1$, otherwise $a_{k,i} = 0$.
$a_{k,j}$	Connection coefficient between central station node k and platform node j , connected if $a_{kj} = 1$, otherwise $a_{kj} = 0$.
С	Corrosion allowance, 2.0.
D D	Diameter of pipeline, mm.
$D_{z,x}, D_{o,x},$	Diameter of injection pipeline <i>z</i> or production pipeline <i>o</i> under condition <i>x</i> , mm.
Е	Axial joint coefficient.
f_{s}	Price of steel, CNY/kg.
F F ^{IC} , F ^{PC}	Total investment of network, CNY. Investment of InNET or ProNET, CNY.
$K_{z,x}$, $K_{o,x}$	Hydraulic coefficient of injection pipeline <i>z</i> or production
112,7,1110,7	pipeline o under condition x.
L	Length of pipeline, km.
L_z , L_o	Length of injection pipeline <i>z</i> or production pipeline <i>o</i> , km. Number of injection or production wells, seats.
N _i C, N _i C P ₁ , P ₂	Starting or ending pressure of pipeline, MPa.
P	Design pressure of pipeline, MPa.
P_z , P_o	Design pressure of injection pipeline z or production pipeline o , MPa.
$p_{\min}^{ ext{IC}}$, $p_{\min}^{ ext{PC}}$	Minimum allowable pressure of InNET or ProNET nodes, MPa.
$p_{ m max}^{ m IC}, \ p_{ m max}^{ m PC}$	Maximum allowable pressure of InNET or ProNET nodes, MPa.
$p_{i,x}^{\mathrm{IC}}$, $p_{i,x}^{\mathrm{PC}}$	Pressure of InNET or ProNET well node i under condition x , MPa.
$p_{j,x}^{\mathrm{IC}}$, $p_{j,x}^{\mathrm{PC}}$	Pressure of InNET or ProNET platform node j under condition x , MPa.
$p_{k,x}^{\text{IC}}, p_{k,x}^{\text{PC}}$	Gas pressure of InNET or ProNET central station node k under condition x , MPa.
$p_{z,1,x}$,	Starting pressure of injection pipeline <i>z</i> or production pipeline <i>o</i> under condition <i>x</i> , MPa.
$p_{o,1,x}$ $p_{z,2,x}$,	Ending pressure of injection pipeline z or production pipeline o
$p_{o,2,x}$	under condition x, MPa.
$q^{\rm IC}$, $q^{\rm PC}$	Injection or production capacity per well, m ³ /d.
$q_{v} \ q_{i,x}^{IC}$	Pipeline flow, m^3/d . Injection flow of well node i under condition x , m^3/d .
$q_{j,x}^{IC}$	Injection flow of platform node j under condition x , m^3/d .
$q_{k,x}^{IC}$	Injection flow of central station node k under condition x , m^3/d .
$q_{i,x}^{PC}$	Production flow of well node i under condition x , m^3/d .
$q_{j,x}^{PC}$	Production flow of platform node j under condition x , m^3/d .
$q_{k,x}^{PC}$	Production flow of central station node k under condition x , m^3/d .
Q ^{IC}	Injection capacity of UNGS, m ³ /d.
Q^{PC}	Production capacity of UNGS, m ³ /d.
Q ^{EPC}	Emergency production capacity of UNGS, m ³ /d.
Q^{PPC} $Q_{z,x}, Q_{o,x}$	Peak production capacity of UNGS, m^3/d . Gas flow of injection pipeline z or production pipeline o under
Q2,X1 Q0,X	condition x , m^3/d .
$Q_{ji,x}^{IC}$	Gas flow of injection pipeline (j, i) under condition x , m^3/d .
$Q_{ki,x}^{IC}$	Gas flow of injection pipeline (k, i) under condition x , m^3/d .
$Q_{kj,x}^{IC}$	Gas flow of injection pipeline (k,j) under condition x , m^3/d .
$Q_{ij,x}^{PC}$	Gas flow of production pipeline (i,j) under condition x , m^3/d .
$Q_{ik,x}^{PC}$	Gas flow of production pipeline (i, k) under condition x , m^3/d .
$Q_{jk,x}^{PC}$	Gas flow of production pipeline (j, k) under condition x , m^3/d .
R t ^{IC}	Minimum yield strength, MPa. Number of injection days, d.
t ^{EPC}	Number of emergency production days, d.
t ^{PPC}	Number of peak production days, d.
T T_z , T_o	Average thermodynamic temperature of gas, K. Average temperature of injection pipeline <i>z</i> or production
2, 0	pipeline o, K.
$v_{z,\min}$,	Minimum allowable flow velocity of injection pipeline z or production pipeline o , m/s.
$v_{o,min}$ $v_{z,x}, v_{o,x}$	Flow velocity of injection pipeline z or production pipeline o
_, 0,	under condition x , m/s .
	(continued on next nage)

(continued on next page)

(continued)

$v_{z, ext{max}}, \ v_{o, ext{max}} \ V^{ ext{PPC}}$	Maximum allowable flow velocity of injection pipeline z or production pipeline o , m/s. Peak production volume, m^3 .
V^{EPC}	Emergency production volume, m ³ .
Z	Compressibility coefficient of gas at average pressure and temperature.
Z_z , Z_0	Compressibility coefficient of injection pipeline <i>z</i> or production pipeline <i>o</i> .
Δ	Relative gas density.
Δ_z , Δ_o	Relative gas density of injection pipeline z or production pipeline o .
ϕ	Strength design coefficient.
σ_T	Temperature reduction coefficient, σ_T to be taken as 1.0 when temperature is below 120 °C.
$ ho_{s}$	Density of steel, kg/m ³ .
λ_z , λ_o	Hydraulic friction coefficient of injection pipeline z or production pipeline o .

Decision variables

- d Pipeline inner diameter, mm.
- d_{ZX} , Inner diameter of injection pipeline z or production pipeline o under
- $d_{o,x}$ condition x, mm.
- η Wall thickness of pipeline, mm.
- η_{zx} , Wall thickness of injection pipeline z or production pipeline o under η_{ox} condition x, mm.

References

- Abadie, J., Carpentier, J., 1969. Generalization of the Wolfe reduced gradient method to the case of nonlinear constraints. Optimization 37–47. https://cir.nii.ac.jp/crid/1572543024699580800.
- Arai, Y., Koizumi, A., Inakazu, T., Koo, J., 2009. Optimization model for water distribution network considering minimization of total replacement cost and stabilization of flow velocity in pipelines. Desal. Water Treat. 2 (1–3), 45–51. https://doi.org/10.5004/dwt.2009.149.
- Arsegianto, A., Soewono, E., Apri, M., 2003. Non-linear optimization model for gas transmission system: a case of Grissik-Duri pipeline. SPE Asia Pacific Oil and Gas Conference and Exhibition. https://doi.org/10.2118/80506-MS.
- Babu, B.V., Chakole, P.G., Mubeen, Syed, Syed Mubeen, J.H., 2005. Differential evolution strategy for optimal design of gas transmission network. Multidiscip. Model. Mater. Struct. 1 (4), 315–328. https://doi.org/10.1163/157361105774501665.
- Chan, A.L.S., Hanby, V.I., Chow, T.T., 2007. Optimization of distribution piping network in district cooling system using genetic algorithm with local search. Energy Convers. Manag. 48 (10), 2622–2629. https://doi.org/10.1016/ j.enconman.2007.05.008.
- Chebouba, A., Yalaoui, F., Smati, A., Amodeo, L., Younsi, K., Tairi, A., 2009. Optimization of natural gas pipeline transportation using ant colony optimization. Comput. Oper. Res. 36 (6), 1916–1923. https://doi.org/10.1016/j.cor.2008.06.005.
- Chen, S.Y., Zhang, Q., Wang, G., Zhu, L.J., Li, Y., 2018. Investment strategy for underground gas storage based on real option model considering gas market reform in China. Energy Econ. 70, 132–142. https://doi.org/10.1016/j.eneco.2017.12.034.
- Deb, K., Pratap, A., Agarwal, S., Meyarivan, T., 2002. A fast and elitist multiobjective genetic algorithm: NSGA-II. IEEE Trans. Evol. Comput. 6 (2), 182–197. https:// doi.org/10.1109/4235.996017.
- Du, X.P., Liu, M.L., Qiu, S., Wu, J.T., Meng, X.Y., 2023. Implications of the European gas market for the long-term construction of underground gas storage in China. Energy Sci. Eng. 11 (6), 2137–2155. https://doi.org/10.1002/ese3.1444.
- El-Mahdy, O.F.M., Ahmed, M.E.H., Metwalli, S., 2010. Computer aided optimization of natural gas pipe networks using genetic algorithm. Appl. Soft Comput. 10 (4), 1141–1150. https://doi.org/10.1016/j.asoc.2010.05.010.
- El-Shiekh, T.M., 2013. The optimal design of natural gas transmission pipelines. Energy Sources, Part B 8 (1), 7–13. https://doi.org/10.1080/15567240802534193.
- Fan, J.J., Wang, J.L., Liu, M.M., Sun, W.M., Lan, Z.X., 2022. Scenario simulations of China's natural gas consumption under the dual-carbon target. Energy 252, 124106. https://doi.org/10.1016/j.energy.2022.124106.
- Hassan, W.H., Attea, Z.H., Mohammed, S.S., 2020. Optimum layout design of sewer networks by hybrid genetic algorithm. J. Appl. Water Eng. Res. 8 (2), 108–124. https://doi.org/10.1080/23249676.2020.1761897.
- IEA, 2023. Medium-Term Gas Report 2023. IEA, Paris. https://www.iea.org/reports/medium-term-gas-report-2023,License:CCBY4.0.
- Jelušič, P., Kravanja, S., Žlender, B., 2019. Optimal cost and design of an underground

- gas storage by ANFIS. J. Nat. Gas Sci. Eng. 61, 142–157. https://doi.org/10.1016/i,jngse.2018.11.003.
- Jia, A.L., Cheng, G., Chen, W.Y., Li, Y.L., 2023. Forecast of natural gas supply and demand in China under the background of "Dual Carbon Targets." Petrol. Explor. Dev. 50 (2), 492–504. https://doi.org/10.1016/S1876-3804(23)60404-5.
- Kabirian, A., Hemmati, M.R., 2007. A strategic planning model for natural gas transmission networks. Energy Policy 35 (11), 5656–5670. https://doi.org/ 10.1016/j.enpol.2007.05.022.
- Liang, Y.T., Zheng, J.Q., Wang, B.H., Zheng, T.C., Xu, N., 2020. Optimization design of natural gas pipeline based on a hybrid intelligent algorithm. Recent Trends in Intelligent Computing, Communication and Devices: Proceedings of ICCD 2018. Springer, Singapore, pp. 1015–1025. https://doi.org/10.1007/978-981-13-9406-5 121
- Peng, S.B., Liu, E.B., Xian, W.W., Wang, D., 2015. Dynamic simulation of an underground gas storage injectionproduction network. J. Environ. Biol. 36 (4), 799–806. https://www.researchgate.net/publication/282048558.
- Srivastava, S.K., Kumar, R., Dikshit, P.K.S., 2015. Optimization of pipe network design using genetic algorithm. i-Manager's. J. Civ. Eng. 5 (2), 31–38. https://doi.org/10.26634/ice.5.2.3352
- Storn, R., Price, K., 1997. Differential evolution—a simple and efficient heuristic for global optimization over continuous spaces. J. Global Optim. 11, 341–359. https://doi.org/10.1023/A:1008202821328.
- Syed, Z., Lawryshyn, Y., 2020. Risk analysis of an underground gas storage facility using a physics-based system performance model and Monte Carlo simulation. Reliab. Eng. Syst. Saf. 199, 106792. https://doi.org/10.1016/j.ress.2020.106792.
- Tian, Q.H., Zhao, D.Y., Zhu, Q.M., 2016. Robust optimization for CO2 pipeline design based on improved parallel co-evolution genetic algorithm. 2016 35th Chinese Control Conference, pp. 9748–9752. https://doi.org/10.1109/ChiCC.2016.7554902.
- Üster, H., Dilaveroğlu, Ş., 2014. Optimization for design and operation of natural gas transmission networks. Appl. Energy 133, 56–69. https://doi.org/10.1016/j.apenergy.2014.06.042.
- Wang, B.H., Liang, Y.T., Yuan, M., Wang, J.H., Zhang, H.R., Li, X.J., 2018. Optimal design of oilfield surface pipeline networks for the cyclic water injection development method. J. Petrol. Sci. Eng. 171, 1400–1408. https://doi.org/ 10.1016/j.petrol.2018.08.065.
- Wang, X.L., Economides, M.J., 2012. Purposefully built underground natural gas storage. J. Nat. Gas Sci. Eng. 9, 130–137. https://doi.org/10.1016/j.jngse.2012.06.003.
- Wei, L.X., Dong, H., Zhao, J., Zhou, G., 2016. Optimization model establishment and optimization software development of gas field gathering and transmission pipeline network system. J. Intell. Fuzzy Syst. 31 (4), 2375–2382. https:// doi.org/10.3233/JIFS-169078.
- Wei, X.X., Shi, X.L., Li, Y.P., Liu, H.J., Li, P., Ban, S.N., Liang, X.P., Zhu, S.J., Zhao, K., Yang, K., Huang, S., Yang, C.H., 2023. Advances in research on gas storage in sediment void of salt cavern in China. Energy 284, 129243. https://doi.org/10.1016/j.energy.2023.129243.
- Wu, X., Li, C.J., Jia, W.L., He, Y.F., 2014. Optimal operation of trunk natural gas pipelines via an inertia-adaptive particle swarm optimization algorithm. J. Nat. Gas Sci. Eng. 21, 10–18. https://doi.org/10.1016/j.jngse.2014.07.028.
- Xu, G.Y., Chen, Y.Q., Yang, M.G., Li, S., Marma, K.J.S., 2023. An outlook analysis on China's natural gas consumption forecast by 2035: applying a seasonal forecasting method. Energy 284, 128602. https://doi.org/10.1016/ j.energy.2023.128602.
- Xue, W.D., Wang, Y., Chen, Z., Liu, H., 2023. An integrated model with stable numerical methods for fractured underground gas storage. J. Clean. Prod. 393, 136268. https://doi.org/10.1016/j.jclepro.2023.136268.
- Xue, W.D., Wang, Y., Liang, Y.J., Wang, T.F., Ren, B.W., 2024. Efficient hydraulic and thermal simulation model of the multi-phase natural gas production system with variable speed compressors. Appl. Therm. Eng. 242, 122411. https:// doi.org/10.1016/j.applthermaleng.2024.122411.
- Yang, C.H., Wang, T.T., Qu, D.A., Ma, H.L., Li, Y.P., Shi, X.L., Daemen, J.J.K., 2016. Feasibility analysis of using horizontal caverns for underground gas storage: a case study of Yunying salt district. J. Nat. Gas Sci. Eng. 36, 252–266. https://doi.org/10.1016/j.jngse.2016.10.009.
- Yu, W.C., Min, Y., Huang, W.H., Wen, K., Zhang, Y., Gong, J., 2018. An integration method for assessing the operational reliability of underground gas storage in a depleted reservoir. J. Pressure Vessel Technol. 140 (3), 031701. https://doi.org/ 10.1115/1.4039070.
- Zhan, H., Yang, J.J., Ding, Y.C., 2012. Improved genetic algorithm for optimization of multi-source pumping tree-type pipe network. Adv. Mater. Res. 402, 738–741. https://doi.org/10.4028/www.scientific.net/AMR.402.738.
- Zhang, G.X., Li, B., Zheng, D.W., Ding, G.S., Wei, H., Qian, P.S., Li, C., 2017. Challenges to and proposals for underground gas storage (UGS) business in China. Nat. Gas. Ind. B. 4 (3), 231–237. https://doi.org/10.1016/j.ngib.2017.07.025.
- Zhang, H.R., Liang, Y.T., Ma, J., Shen, Y., Yan, X.H., Yuan, M., 2017. An improved PSO method for optimal design of subsea oil pipelines. Ocean Eng. 141, 154–163. https://doi.org/10.1016/j.oceaneng.2017.06.023.
- Zhang, Z.W., Liu, X.T., 2017. Study on optimal operation of natural gas pipeline network based on improved genetic algorithm. Adv. Mech. Eng. 9 (8), 1687814017715981. https://doi.org/10.1177/1687814017715981.
- Zhao, L., Yan, Y.F., Wang, P., Yan, X.Z., 2019. A risk analysis model for underground gas storage well integrity failure. J. Loss Prevent. Process Ind. 62, 103951. https:// doi.org/10.1016/j.jlp.2019.103951.
- Zheng, Y.L., Sun, J.C., Qiu, X.S., Lai, X., Liu, J.D., Guo, Z.P., Wei, H., Min, Z.S., 2020.

- Connotation and evaluation technique of geological integrity of UGSs in oil/gas fields. Nat. Gas. Ind. B. 7 (6), 594–603. https://doi.org/10.1016/j.ngib.2020.05.002.
- Zheng, Z.W., Wu, C.C., 2012. Power optimization of gas pipelines via an improved particle swarm optimization algorithm. Pet. Sci. 9, 89–92. https://doi.org/10.1007/s12182-012-0187-8.
- Zhou, J., Fu, T.T., Chen, Y.L., Xiao, Y., Peng, J.H., Liang, G.C., 2021a. A mixed integer nonlinear programming model for optimal design of natural gas storage surface double-pipe network. J. Energy Storage 44, 103379. https://doi.org/10.1016/j.est.2021.103379.
- Zhou, J., Liang, G.C., Deng, T., 2018. Optimal design of star-tree oil-gas pipeline network in discrete space. J. Pipeline Syst. Eng. Pract. 9 (1), 04017034. https:// doi.org/10.1061/(ASCE)PS.1949-1204.0000302.
- Zhou, J., Zhou, L.L., Liang, G.C., Wang, S.B., Fu, T.T., Zhou, X., Peng, J.H., 2021b. Optimal design of the gas storage surface pipeline system with injection and withdrawal conditions. Petroleum 7 (1), 102–116. https://doi.org/10.1016/j.petlm.2020.05.003.
- Zhou, J., Zhou, X., Liang, G.C., Peng, J.H., 2020. An MINLP model for network layout of underground natural gas storage. J. Intell. Fuzzy Syst. 38 (4), 4619–4642. https://doi.org/10.3233/JIFS-191383.
- Zhou, J., Zhao, Y.X., Fu, T.T., Zhou, X., Liang, G.C., 2022. Dimension optimization for underground natural gas storage pipeline network coupling injection and production conditions. Energy 256, 124651. https://doi.org/10.1016/ j.energy.2022.124651.
- Zhou, M., Zhang, Y., Jin, S.J., 2015. Dynamic optimization of heated oil pipeline operation using PSO–DE algorithm. Measurement 59, 344–351. https://doi.org/ 10.1016/j.measurement.2014.09.071.
- Zlender, B., Kravanja, S., 2011. Cost optimization of the underground gas storage. Eng. Struct. 33 (9), 2554–2562. https://doi.org/10.1016/j.engstruct.2011.05.001.
- Zou, C.N., Chen, Y.P., Kong, L.F., Sun, F.J., Chen, S.S., Dong, Z., 2019. Underground coal gasification and its strategic significance to the development of natural gas industry in China. Petrol. Explor. Dev. 46 (2), 205–215. https://doi.org/10.1016/S1876-3804(19)60002-9.